UNITED STATES DEPARTMENT OF THE INTERIOR

GEOLOGICAL SURVEY

Eruptive History, Petrology, and Petrogenesis of the Joe Lott Tuff Member of the Mount Belknap Volcanics, Marysvale Volcanic Field, West-Central Utah

By

Karin E. Budding

Open-File Report 82-891
1982

CONTENTS

ILLUSTRATIONS

PLATE

TABLES

PREFACE

Joseph Augustus Lott, born March 10, 1855, was one of nine children of John Smiley Lott and his two wives, Mary Ann Faucett and Docia Emmerine Molen. John Lott was a soldier and settler for the Mormon Church. The Lott cabin, built by John in the mid-1870's, is located in Clear Creek Canyon and represents a pioneer lifestyle common during Utah's territorial period. The homestead is significant because of its location on the Old Spanish Trail which is a major trade route connecting the Great Basin with Nevada and California. The cabin, now in the path of I-70, was surrounded by cottonwoods and a variety of fruit trees. The Lott's economic survival depended on the production of grains, vegetables, fruit, and stock for home consumption.

Joseph Lott married Marua Twitchell on May 18, 1878 and had four daughters and six sons. They settled in Clear Creek Canyon and farmed. In addition, Joe drove a wagon train up to the miners at the gold and silver mine at Kimberly delivering mail and supplies. Presumably because of this work, the rocks forming the walls of Clear Creek Canyon are known as the Joe Lott Tuff Member of the Mount Belknap Volcanics.

ABSTRACT

The Joe Lott Tuff Member of the Mount Belknap Volcanics is the largest rhyolitic ash-flow tuff sheet in the Marysvale volcanic field. It was erupted 19 m.y. ago, shortly after the changeover from intermediate-composition calc-alkalic volcanism to bimodal basalt-rhyolite volcanism. Eruption of the tuff resulted in the formation of the Mount Belknap Caldera whose pyroclastic intracaldera stratigraphy parallels that in the outflow facies. The Joe Lott Tuff Member is a composite ash-flow sheet that changes laterally from a simple cooling unit near the source to four distinct cooling units toward the distal end. The lowest of these units is the largest and most widespread; it is 64 m thick and contains a basal vitrophyre. Eruption of the lower unit led to the initial collapse of the caldera. The lower unit is followed upward by a 43 m middle unit, a 26 m pink-colored unit which is separated by a prominent air-fall layer, and a 31 m upper unit.

The Joe Lott Tuff Member is an alkali rhyolite with 75.85-77.31 wt.% silica and 8.06-9.32 wt.% K_2O+Na_2O; the agpaitic index ($Na_2O+ K_2O/Al_2O_3$) is .77-.98. The tuff contains about 1% phenocrysts of quartz, sanidine, oligoclase, augite, apatite, zircon, sphene, biotite, and oxidized Fe-Ti oxides. The basal vitrophyre contains accessory allanite, chevkinite, and magnesiohastingsite. The main cooling units are chemically and mineralogically zoned indicating that the magma chamber restratified prior to each major eruption. Within each of the two thickest cooling units, the mineralogy changes systematically upwards; the Or content and relative volume of sanidine decreases and An content of plagioclase increases. The basal vitrophyre of the lower unit has a bulk composition that lies in the thermal trough near the minima of Or-Ab-Q at 1 kb pH_2O. Microprobe analyses of feldspar and chemical modeling on experimental systems indicate that pre-eruption temperatures were near 750°C and that the temperature increased during the eruption of the cooling units.

The chemical gradients in the apatite and whole-rock data in the Joe Lott Tuff Member and the consistent mineral assemblages throughout the ash-flow cannot be explained by crystal settling. The fractionation of the Joe Lott Tuff Member appears to closer fit the model of convection-driven thermogravitational diffusion.

INTRODUCTION

General

It has long been known that large-volume silicic magma chambers are zoned chemically and thermally. Ash-flow tuffs resulting from caldera-forming eruptions represent the rapidly quenched magma chamber in inverted order. Compositional analyses of these rocks give insight into the vertical variations in chemistry and temperature in the chamber immediately prior to eruption, and enable interpretation of the processes of fractionation causing the zonation. Commonly with increasing depth in the chamber, the phenocryst content increases while the magma becomes more mafic as is evident in the Bandelier Tuff, New Mexico (Smith and Bailey, 1966), and in the Paintbrush Tuff, Nevada (Lipman and others, 1966).

Recent work by Shaw and others (1976) and Hildreth (1976, 1977, 1979, 1981) has shed new light on fractionation processes in high-level silicic magma chambers. Detailed chemical analyses of large ash-flow sheets, particularly the Bishop Tuff, California, yielded systematic chemical gradients that cannot be explained by the more conventional fractionation processes of crystal-liquid differentiation or partial melting. The strong gradients seen in the minor and trace elements are accompanied by very small changes in the major element chemistry. A mechanism which apparently explains the fractionation trends observed in the Bishop Tuff is termed convection-driven thermogravitational diffusion (Hildreth, 1976). Briefly, this involves the fractionation of a magma in its liquid state, predominantly by liquid state thermodiffusion, volatile complexing, and convection due to the addition of heat from basalt intruding below. A gravitationally stable zone of volatile-rich magma develops at the top of the chamber reflecting gradients in temperature and volatile content near the interface of the magma with the wall and roof rocks. The combined effects of these gradients and the resultant variations in the degree of polymerization of the melt in the roof zone produces the observed elemental enrichments and depletions depending on the nature of the ionic complexes each element forms.

Other studies of the products of silicic volcanism and plutonism yield major, minor, and trace element chemical gradients very similar to those found in the Bishop Tuff. These include studies of the Bandelier Tuff, New Mexico (Smith, 1979); Sierra La Primavera, Jalisco, Mexico (Mahood, 1981); Coso Volcanic Field, California (Bacon, 1981); Twin Peaks, Utah (Crecraft and others, 1981); and the Redskin Granite, Colorado (Ludington, 1981). Fractionation in a liquid state by thermogravitational diffusion appears to be a viable mechanism in each case.

Purpose of the study

The Mount Belknap Volcanics in the Marysvale volcanic field of west-central Utah is composed of hundreds of cubic kilometers of silicic alkali rhyolite lava domes, lava flows, and ash-flow tuffs. The Mount Belknap Caldera collapsed approximately 19 m.y. ago with the eruption of approximately 150 km^3 of ash called the Joe Lott Tuff Member. As the Joe Lott Tuff Member represents the bulk of the erupted portion of the Mount Belknap magma chamber in its quenched, inverted form, it is likely to contain information critical to understanding the fractionation processes active in the chamber prior to the ash-flow eruptions.

This study of the eruptive history of the Joe Lott Tuff Member began with the mapping of the cooling units at a scale of 1:24,000. Chemical analyses of the whole-rock samples and electron microprobe analyses of the phenocrysts followed in order to unravel the chemical evolution of the magma chamber. The work was done with the guidance of Charles G. Cunningham and Thomas A. Steven, U.S. Geological Survey, who, in the past seven years, have been actively working in the Marysvale area unraveling the volcanic history of the field, evaluating the mineral resource potential, and developing models for the origin of the base and precious metals found there.

This study was undertaken to partially fulfill the requirements for the Master of Science degree at the University of Colorado in Boulder. I gratefully acknowledge the members of my committee, Charles Stern, Ed Larsen, and Charles Cunningham, for their continuous assistance and support.

GEOLOGIC SETTING

Regional geology

Marysvale, Utah, is located in the north-trending Marysvale Valley 260 km south of Salt Lake City, within the Marysvale volcanic field (fig. 1). The field, which covers more than 2,000 km^2 in west-central Utah, lies in the High Plateaus physiographic subprovince which forms the transition between the Colorado Plateau province to the east and the Basin and Range province to the west. The Marysvale Valley, at an elevation of 2,000 m, is bordered on the west by the Tushar Mountains (elevation 3,700 m) and on the east by the Sevier Plateau at 2,900 m.

The volcanic rocks in the Marysvale area lie unconformably on Mesozoic and lower Cenozoic sedimentary rocks. Most of the volcanic rocks in the pile are 35- to 22-m.y.-old intermediate composition, calc-alkalic lava flows, volcanic breccias, volcaniclastic deposits, and ash-flow tuffs which form the Bullion Canyon Volcanics. These rocks accumulated around many scattered and partially clustered stratovolcanoes. Quartz monzonite stocks intruded vent-facies rocks in the cores and flanks of some of these intermediate-composition volcanoes about 23 m.y. ago near the end of intermediate composition volcanic activity. Local thicknesses of the Bullion Canyon Volcanics range from 100 to 200 m; however, deposits greater than 1 km thick are found near the center of the area (Steven and others, 1979).

The composition of the volcanic rocks changed abruptly around 21 m.y. ago to a bimodal basalt-rhyolite assemblage, coinciding with the beginning of extensional basin and range tectonism in adjacent parts of the Great Basin. Subsequently, a much greater volume of the rhyolitic end member was erupted. Silicic alkali rhyolite lava domes, lava flows, and ash-flow tuffs were extruded from two source areas; the Mount Belknap caldera, 20 km west of Marysvale forms the western source area, and the domes, lava flows, small stocks, and ash-flow tuffs from the Red Hills caldera and the Alunite Ridge area, from about 9 km northeast of Marysvale to about 12 km southwest of Marysvale, form the eastern source area (fig. 1). Both areas were located over high level magma chambers. The difference in eruptive history of the two areas may have been caused by the different shape and depth of the magma chambers (Cunningham and Steven, 1979). These two calderas and their outflow are part of the Mount Belknap Volcanics and at one time covered an area

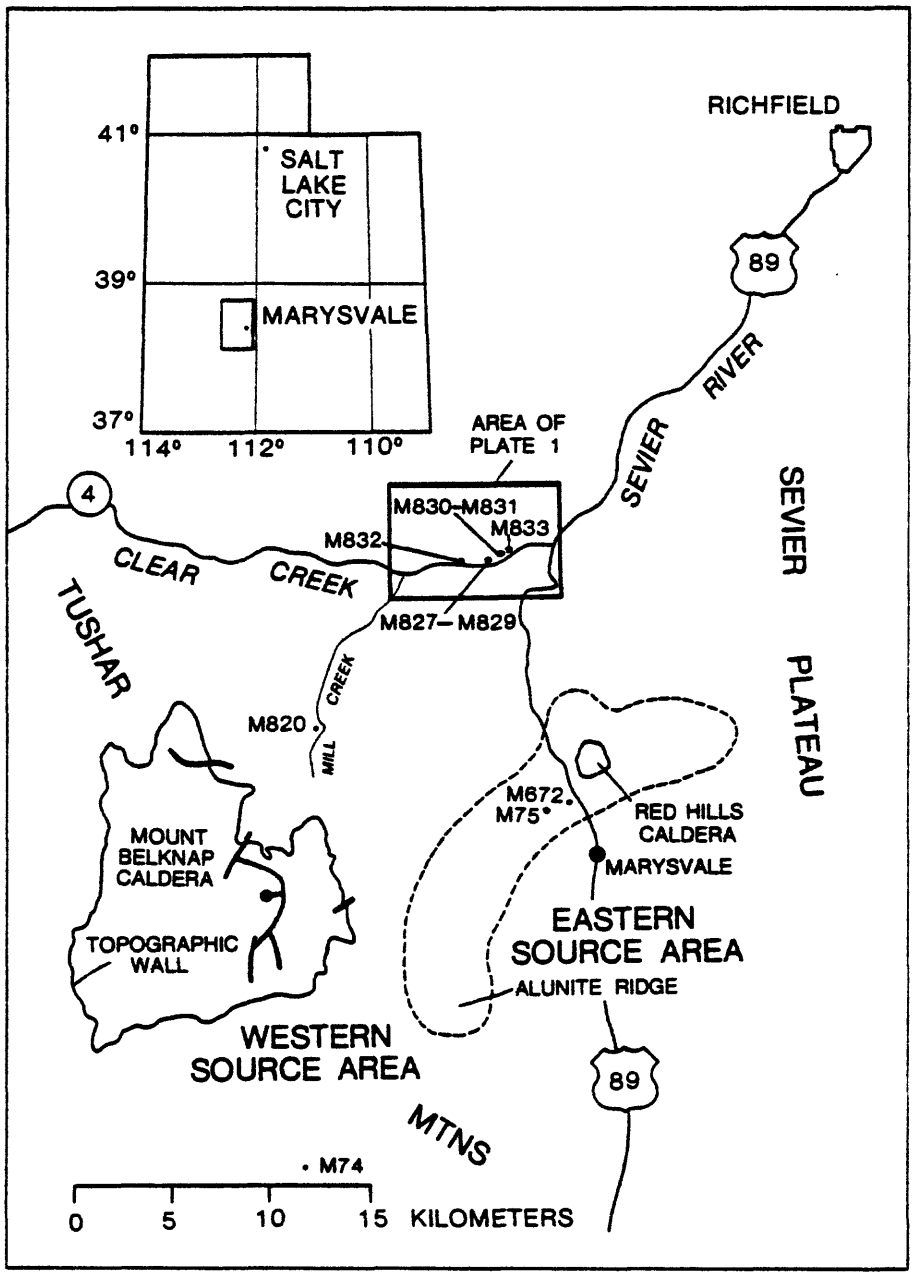

Figure 1.--Index map showing the location of the western and eastern source areas of the Mount Belknap Volcanics, the Mount Belknap and Red Hills Calderas, the area mapped in detail for this study (plate 1), sample localities, and principal geographic features mentioned in the text.

greater than 600 km^2--the bulk being erupted from the western source area. The Mount Belknap caldera formed as a result of the eruption of the Joe Lott Tuff Member and the Red Hills caldera formed as a result of the eruption of the Red Hills Tuff Member. Both calderas formed about 19 m.y. ago. Igneous activity producing later parts of the Mount Belknap Volcanics continued in the western source area until around 16 m.y. ago and in the eastern source area until about 14 m.y. ago (Cunningham, Steven, and Naeser, 1982).

Basin and Range faulting in the Marysvale area possibly began as early as 22 m.y. ago and continued through most of remaining Cenozoic time. The Miocene and Pliocene Sevier River Formation, consisting of fluviatile and minor lacustrine sediments, was deposited in basins developed concurrently with the faulting. Many local ash-fall tuffs within the Sevier River Formation indicate that episodic volcanic activity occurred in the area during this period of sedimentation. Tholeiitic basalt flows of low volume erupted widely and are locally interleaved with the Sevier River sediments (Steven and others, 1979). An upper Tertiary rhyolite dome in the southern Sevier Plateau dated at 5.4 m.y. helps constrain the age of development of the present physiography (Rowley and others, 1981).

Mount Belknap Caldera

The Mount Belknap Caldera is located in the central Tushar Mountains. The source area is in hilly terrain of eroded remnants of a cluster of Bullion Canyon central-vent volcanoes. Minor premonitory eruptions occurred before the catastrophic eruption of many tens of cubic kilometers of ash-flow tuff, the largest amount forming the Joe Lott Tuff Member, which resulted in the subsequent caldera collapse. Large-volume eruptions took place during and immediately after subsidence; however, most activity occurred in a short time span, within the analytical uncertainty of 18.3±1.1 m.y. The caldera fill consists of rhyolite ash-flow tuffs, viscous lava flows, lava domes, and volcanic breccias. There is no evidence of resurgence in the caldera; rather the central region has subsided a maximum of 150 m as a tilted trapdoor block (Cunningham and Steven, 1979).

The irregularly shaped caldera is 13 km wide east-west and 17 km long north-south. Based on the structural margin, the high-level magma chamber is thought to have been broad (at least 10 km across) with the subsided block being about 9 to 10 km across. A water pressure of 800±200 bars in the magma is obtained from plotting the average normative mineral compositions (Q-Or-Ab) of the Joe Lott Tuff Member (Cunningham and Steven, 1979) on the quaternary system Q-Or-Ab-H_2O (Tuttle and Bowen, 1958). This pressure represents an equivalent lithostatic depth of 3 to 4 km, which is thought to be a realistic distance to the top of the magma prior to eruption (Cunningham and Steven, 1979).

The erupted ash-flow volume of 150 km^3 for the Joe Lott Tuff Member fills a cone-shaped body that is 1.9 km deep. The top of the cone has a surface area of 148 km^2, based on the area of the caldera, and tapers downward at a 45^o angle to a surface area of 78 km^2, based on the structural margin of the subsided block. Smith (1979) has developed a model illustrating the probable relationship between the volume of pyroclastic eruptions and the assumed thickness of the derivative magma. This magma gains it mobility from the thermal source provided by the underlying more mafic, probably mantle derived

magma. When the erupted ash-flow volume of 150 km^3 for the Joe Lott Tuff Member is plotted on the model, a depth of approximately 4 km is obtained for the top of the magma chamber down to an interface with the primitive magma. The maximum depth below the roof zone from which material is erupted for a magma chamber of this volume is 1.8 km. This correlates well with the depth of eruption calculated from field evidence.

Geochronology

Prior to this study, the Joe Lott Tuff Member had not been dated; however, through stratigraphic relationships and from dates on nearby rock units it was determined to be approximately 19 m.y. old. Underlying the Joe Lott Tuff Member, a basal ash-flow tuff (belonging to the lower heterogeneous member of the Mount Belknap Volcanics) gave fission-track ages of 19.6±0.8 m.y. on zircon and 18.8±1.7 m.y. on apatite (Steven and others, 1979). The Red Hills Tuff Member, which overlies the Joe Lott Tuff Member, has a K/Ar age on sanidine of 18.9±0.7 m.y. (Cunningham, Ludwig, and others, 1982).

Two samples of the Joe Lott Tuff Member--the upper unit (M833) and the basal vitrophyre (M820)--were selected for K/Ar dating at the U.S. Geological Survey through the generous assistance of Harald Mehnert and Glen Izett. Sanidine from the upper cooling unit gave a concordant age of 18.3±1.1 m.y. (table 1), thereby verifying the previously considered age.

The basal vitrophyre, on the basis of whole-rock methods, is 17.2±0.7 m.y. old. This age is considered to be too young; it is attributed to a loss of argon related to hydration of the volcanic glass (Dalrymple and Lanphere, 1969). The dull appearance of the vitrophyre indicates it is indeed hydrated.

Joe Lott Tuff Member of the Mount Belknap Volcanics

The Joe Lott Tuff Member is the largest ash-flow tuff erupted in the Mount Belknap Volcanics and its eruption was associated with the collapse of the Mount Belknap Caldera. It is a high silica, crystal-poor alkali rhyolite and is widely distributed around the caldera. Widespread sheets of the tuff north and south of the caldera overlie fairly flat-lying volcaniclastic beds, lava flows, and ash-flow tuffs of the Bullion Canyon Volcanics. Near the source, the tuff is red and dense and forms a simple cooling unit. A lateral transition is evident in color and degree of welding (fig. 2), and in its distal parts, the Joe Lott Tuff Member is gray and forms a compound cooling unit composed of multiple ash-flow tuffs.

The most complete exposure of the compound cooling unit is found west of U.S. Highway 89, along Clear Creek Canyon (fig. 1). Detailed mapping of the Joe Lott Tuff Member done along and to the north of Clear Creek as this covers the largest outcrop area of the ash flow (pl. 1). In Clear Creek Canyon, the Joe Lott Tuff Member overlies the Three Creeks Tuff Member of the Bullion Canyon Volcanics and is overlain by sands and gravels of the Sevier River Formation.

Four cooling units were delineated in the mapping of the Joe Lott Tuff Member which, in stratigraphic succession, include the lower, middle, pink, and upper units (fig. 3). The basal vitrophyre of the lower cooling unit was only found in one locality, approximately 8 km south of Clear Creek Canyon

Table 1.--Data for K/Ar ages of the Joe Lott Tuff Member

Sample	Lab Number	Material	K_2O%	$^{40}Ar^*$ (10^{-10} moles/g)	% radiogenic argon	Age in m.y. ±2
M833	DKA4127	Sanidine	5.56, 5.68[1]	1.487	61.3	18.3±1.1
M820	DKA4126	Obsidian	4.83, 4.85[1]	1.204	68.6	17.2±0.7

[1]Determined by flame photometry.

Decay constants for ^{40}K

$\lambda_\varepsilon + \varepsilon' = 0.581 \times 10^{-10}$/yr

$\lambda_\beta = 4.962 \times 10^{-10}$/yr

$^{40}K/K = 1.167 \times 10^{-4}$ atom %

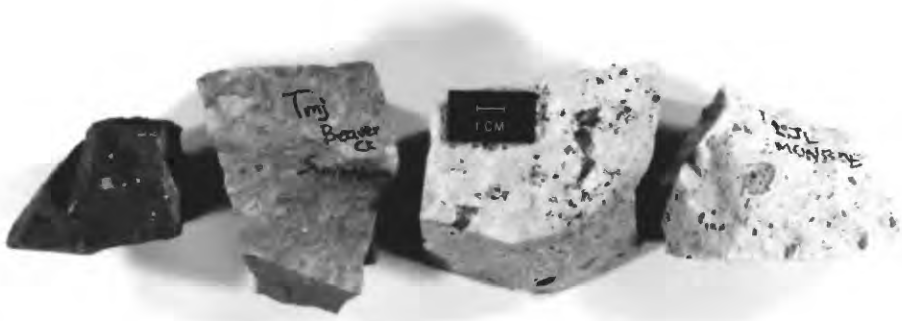

Figure 2.--Hand samples illustrating the lateral transition of the Joe Lott Tuff Member from red, dense rock near the source to gray, poorly welded rock in the distal end of the ash-flow sheet.

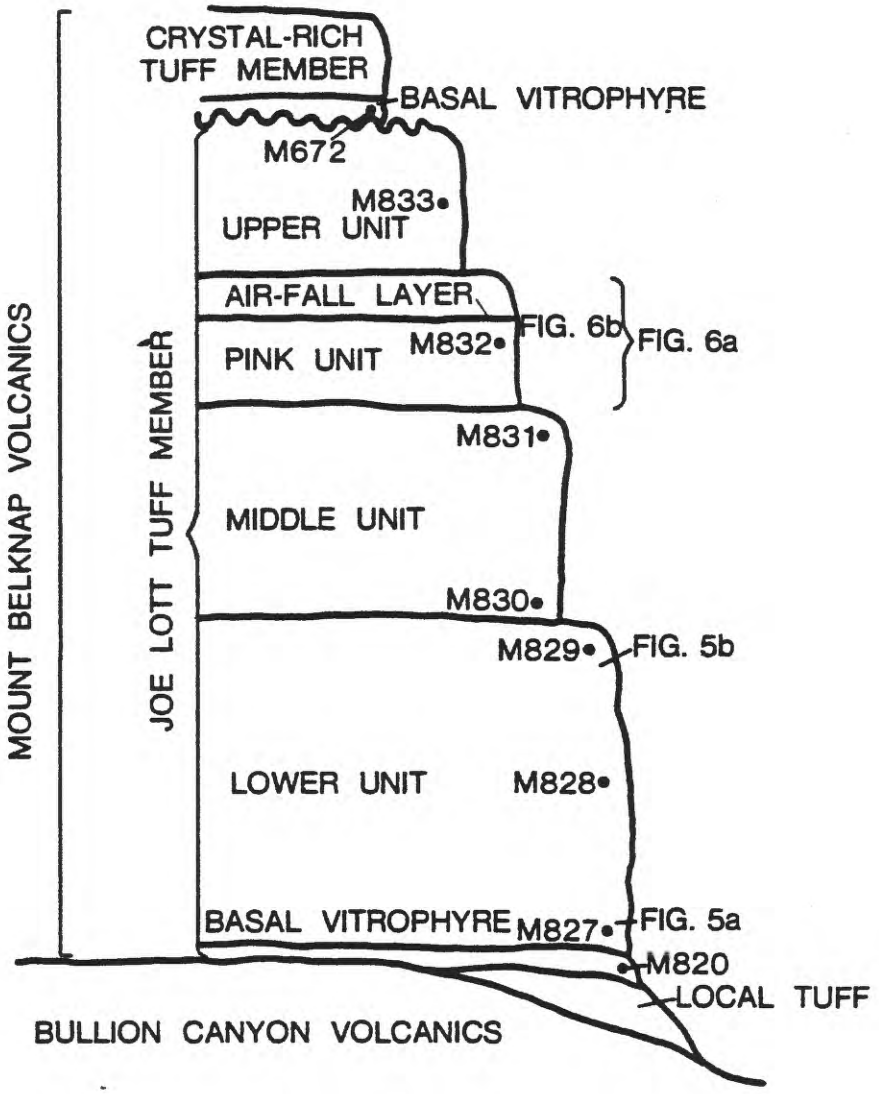

Figure 3.--Diagrammatic sketch of stratigraphic relationship of the Bullion Canyon Volcanics, the lower, middle, pink, and upper units of the Joe Lott Tuff Member, and the crystal-rich tuff member of the Mount Belknap Volcanics. Includes sample and photograph positions, and the portion of the composite sheet seen in figure 4.

along Mill Creek (fig. 1). The black glass has a moderate amount of small, flow-banded rhyolitic lithic fragments. The most complete and impressive exposure of the lower, middle, and upper cooling units is seen on the eastern end of Clear Creek Canyon (fig. 4) where the erosional benches separating the units are clearly defined. The approximate thickness of each cooling unit at this locality is: lower unit, 64 m; middle unit, 43 m; and upper unit, 31 m. The pink unit is more completely exposed farther west in Clear Creek Canyon where it is a maximum of about 26 m thick.

Near the base of the lower cooling unit the tuff is a very densely welded purplish-gray rock with rhyolitic lithic fragments and pumice fragments flattened in the plane of compaction foliation forming fiamme (fig. 5a). The welding has resulted in horizontal platy jointing near the base. Columnar jointing from tensional cooling is present in the bottom part of the unit. The unit grades upward into a poorly welded, purplish-white, somewhat chalky rock bearing devitrified pumice fragments (fig. 5b).

A ground surge deposit is locally present at the bottom of the middle cooling unit. It is approximately 1 m thick, slightly oxidized (pink to light purple in color), and pumice rich. The ash flow near the base of the middle unit is a moderately welded gray rock with small lithic fragments and some pumice clasts which are flattened in the plane of compaction. Columnar jointing is present. Near the top of this unit the rock becomes less welded, lighter in color, and somewhat chalky. Evidence of piping was found in two localities in the middle unit. Here erosion by water from an underground stream percolating along cooling joints has resulted in vertical "pipes" leading to a basal horizontal layer which all contain pinkish, conglomeratic tuffaceous material. The pink color reflects the higher permeability of the rock and increased secondary oxidation.

The pink cooling unit, which lies between the middle and upper units, is poorly welded, easily erodable, pumice rich, and so named because of its prominent pink color. It is discussed in more detail below. The upper cooling unit is gray and poorly welded; it contains small lithic fragments.

Weathering of the tuff produces cavernous features as the softer tuff is eroded from beneath a thin, exterior, iron-stained silicified shell. Secondary halite is locally present.

The pink cooling unit, between the middle and upper cooling units, exhibits distinctive physical features throughout its outcrop area. These include the pink color, the characteristic weathering habit, and an air-fall layer within the unit (fig. 6a). The cooling unit is composed of two poorly to moderately welded ash-flow tuffs separated by a prominent air-fall layer. The ash flows of this unit have a much higher pumice content relative to the other cooling units. The ratio of pumice to rhyolitic lithic fragments is about 10:1 although it is locally quite variable. The pumice fragments are somewhat compacted and some are as much as 8 cm long. Some of the glass in the tuff has devitrified; in some places the tuff has been oxidized to an orange, crumbly material. The pink unit does not develop a resistant iron-oxide weathering rind as do the other cooling units; rather, it erodes into rounded shapes grossly resembling dunes. Cavernous forms also result from the weathering. In places, the unit has been eroded away until it is protected by the upper cooling unit and a wide bench exists at the pink unit/middle unit contact.

Figure 4.--View of the Joe Lott Tuff Member composite sheet, along the eastern end of Clear Creek Canyon, includes the most complete section where the lower, middle, and upper units were measured and sampled.

Figure 5a.--Photograph of the densely welded base of the lower cooling unit of the Joe Lott Tuff Member showing pumice fragments flattened in plane of compaction foliation forming fiamme.

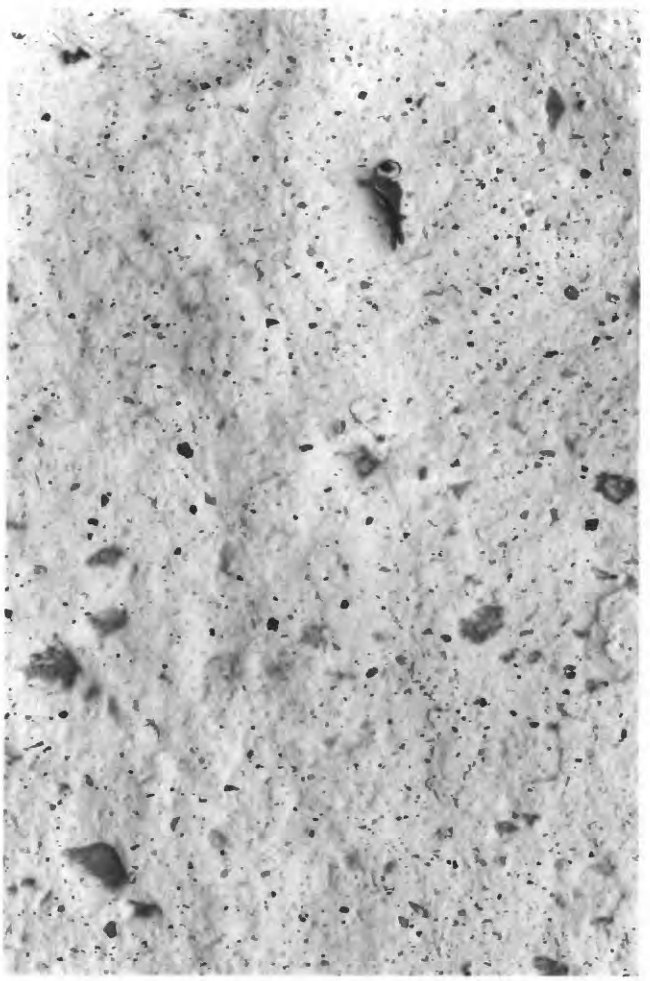

Figure 5b.--A view of the poorly welded top of the lower cooling unit.

Figure 6a.--Photograph of the pink cooling unit of the Joe Lott Tuff Member with the air-fall layer and characteristic cavernous weathering.

The thickness of this cooling unit varies laterally, and in some places is absent. For example, eastward along Clear Creek Canyon the unit thins (maximum of approximately 25 m) until it completely wedges out. At a good exposure along Clear Creek, 4.2 km west of the intersection of Highways 4 and 89, the ash-flow tuff below the air-fall layer is 17 m thick, the air-fall layer is 0.5 m thick, and the ash flow above the air-fall layer is 9 m thick.

The air-fall layer which ranges in thickness from approximately 0.5 m to 1.0 m, contains three prominent graded layers that are exceptionally uniform over a lateral distance of about 2 km (fig. 6b). The upper layer may be subdivided into even thinner graded layers. The laminar layers grade upward from gray to reddish, flow-banded to homogeneous, angular rhyolitic fragments and pumice fragments about 1 cm long into finer fragments of rhyolites, pumice, and obsidian. The pumice clasts are flattened in the plane of compaction foliation, indicating emplacement while hot. The rhyolite fragments may represent a shattered dome or plug at the source. The laminar layers show no signs of crossbedding, scouring, slump features, or other indications of being reworked by water. Locally the air-fall layer overlies a base surge deposit containing fine-grained rhyolite fragments and some pumice (fig. 6c). The base surge deposit shows mantling of topography and is capped by a coarse-grained fragmental rhyolite lag deposit.

The pink color is restricted to this one cooling unit. The color is thought to result from the oxidation of the iron in the ash brought about by the percolation of ground water through the pink unit prior to emplacement of the upper cooling unit. An undulating silica-rich band is present below the air-fall layer near the base of the pink ash flow and probably represents the paleo water table. Montmorillonite is present locally at the base of the pink unit and thought to have formed from the alteration of volcanic ash by water (Millot, 1970). The oxidation and hydration of the pink unit directly correlates with the increased permeability of the poorly welded tuff. The much more densely welded underlying middle unit was not oxidized by the percolating ground water; however, the top 0.5 m of the middle unit is commonly purple, perhaps indicating minor oxidation and suggesting that the unit was not impervious to the effects of the ground water.

Alternatively, the oxidation of the iron causing the pink color in the tuff may have been a high-temperature phenomena caused by the eruption of the unit through an intermittent caldera lake which had waned during the plinian air-fall eruption.

Crystal-rich tuff member of the Mount Belknap Volcanics

The crystal-rich tuff member was erupted from the Mount Belknap Caldera 19.0±1.2 m.y. ago (Steven and others, 1979), and is the only major outflow unit from the caldera other than the Joe Lott Tuff Member which it directly overlies. The moderately welded alkali rhyolite ash-flow tuff fills paleochannels that radiate out from the caldera. The major cooling unit, which is approximately 15 m thick, is overlain by one to two relatively thin cooling units of similar lithology. Each cooling unit contains a basal vitrophyre.

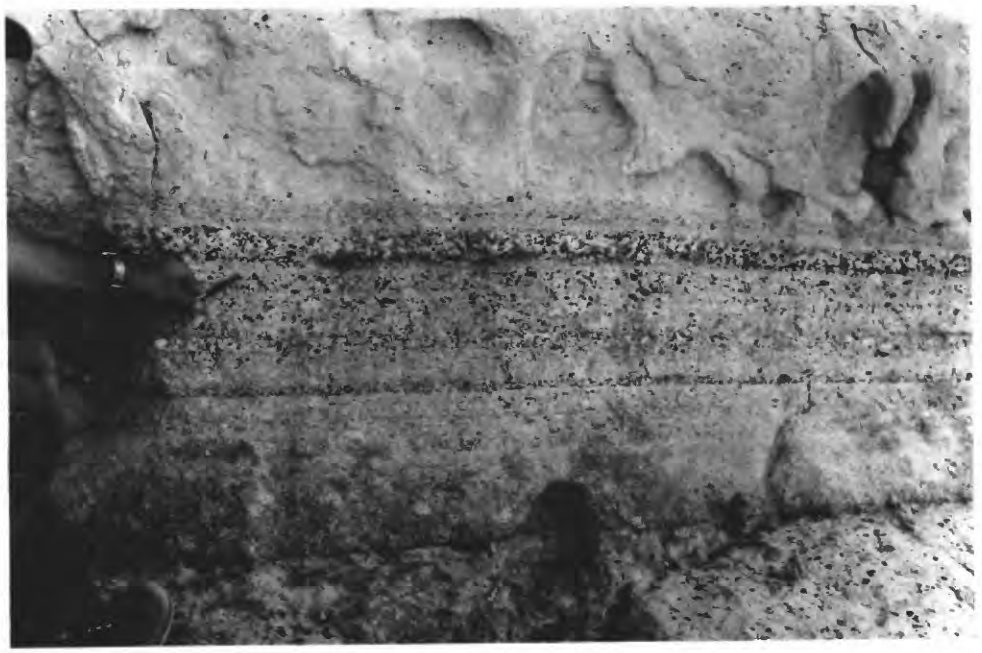

Figure 6b.--Detail of the air-fall layer in the pink cooling unit exhibiting the three graded layers of rhyolite fragments and pumice.

Figure 6c.--Photograph of the base surge deposit and the overlying air-fall layer in the pink cooling unit. Base surge shows mantling of topography.

SAMPLE LOCATIONS AND DESCRIPTIONS

A suite of nine large samples was collected from the Joe Lott Tuff Member and the crystal-rich tuff member to document the character of the magma and phenocryst chemistry of the pre-eruptive magma under the Mount Belknap caldera. Due to the low phenocryst content, high degree of welding, and possible secondary chemical modifications from ground water activity of the Joe Lott Tuff Member, it was not feasible to restrict sample collection to pumice; therefore, a large volume of the fresh whole-rock sample was collected. Four samples, including one from the vitrophyre, were collected from the relatively thick lower cooling unit. Two samples were taken from the thinner middle cooling unit and one sample each from the pink and upper cooling units.

Locations and modal analyses for each of the Joe Lott Tuff Member and crystal-rich tuff member are given in tables 2 and 3. The analyses are based on one thousand points counted exclusive of lithic fragments. Because of the low phenocryst content (less than 1 percent) of the Joe Lott Tuff Member, the statistics of the relative mineral abundance are not significant and only the presence or absence of the mineral is reported. The paucity of the crystals in the Joe Lott Tuff Member indicates that the magma was erupted when very near its liquidus.

All Joe Lott Tuff Member samples have a devitrified groundmass with the exception of the vitrophyre. Spherulitic devitrification is common in the pumice fragments, whereas the glass shards commonly exhibit axiolitic devitrification. Remobilized silica and vapor-phase crystallization of quartz and feldspar has occurred in lithophysal cavities. Compaction of the glass shards varies with stratigraphy. By far the most intensely welded portion is the base of the lower cooling unit (fig. 7). Welding decreases upward in both the lower and middle cooling units, clearly reflecting the decrease in lithostatic load. Rhyolitic lithic fragments are present in the samples to varying degrees.

The primary variations observed in the Joe Lott Tuff Member samples are the different degrees of welding and the slight change in phenocryst content. The quartz and sanidine content increases upward in the lower cooling unit reflecting an increase in crystal content with depth in the magma chamber, a common phenomena of zoned silicic magma chambers (Lipman and others, 1966; Smith, 1979). The concentration of both minerals drops to zero at the base of the middle unit, but quartz content is higher at the top of the middle unit again reflecting greater phenocryst content downward in the chamber, and substantiating the trend seen in the lower unit.

Table 2.--Location of analyzed samples from the Joe Lott Tuff Member and the crystal-rich tuff member

Sample No.	Description	Location
M672	Vitrophyre-crystal-rich tuff member	3.2 km north of Marysvale on U.S. Highway 89
	Joe Lott Tuff Member	
M833	Upper unit	2.0 km west of U.S. Highway 89 on State Road 4
M832	Pink unit	4.2 km west of U.S. Highway 89 on State Road 4
M831	Middle unit - top	2.1 km west of U.S. Highway
M830	Middle unit - bottom	89 on State Road 4
M829	Lower unit - top	
M828	Lower unit - middle	2.9 km west of U.S. Highway
M827	Lower unit - bottom	89 on State Road 4
M820	Vitrophyre	8 km south of State Road 4 along Mill Creek

Table 3.--Modal analyses, in percent, of the Joe Lott Tuff Member and the crystal-rich tuff member

[Presence (+), absence (-)]

Sample	Groundmass	Total Phenocrysts	Quartz	Alkali-Feldspar	Plagioclase	Biotite	Pyroxene	Opaque	Apatite + Zircon
Crystal-rich tuff member,									
vitrophyre (M672)-------	78.1	21.9	15.2	4.7	0.1	0.7	0.5	0.7	-
Joe Lott Tuff Member,									
Upper unit (M833)-------	99.0	1.0	-	-	-	+	-	+	+
Pink unit (M832)--------	99.3	.7	+	-	-	-	-	-	-
Middle unit - top (M831)	99.0	1.0	+	-	-	-	-	+	+
Middle unit - bottom (M830)----------	99.6	.4	-	-	-	-	-	+	-
Lower unit - top (M829)-	96.9	3.1	+	+	-	-	-	+	+
Lower unit - middle (M828)----------	99.3	.7	+	+	-	-	-	+	-
Lower unit - bottom (M827)----------	99.4	.6	-	+	-	-	-	+	-
Vitrophyre (M820)-------	99.7	.3	+	-	-	-	-	+	-

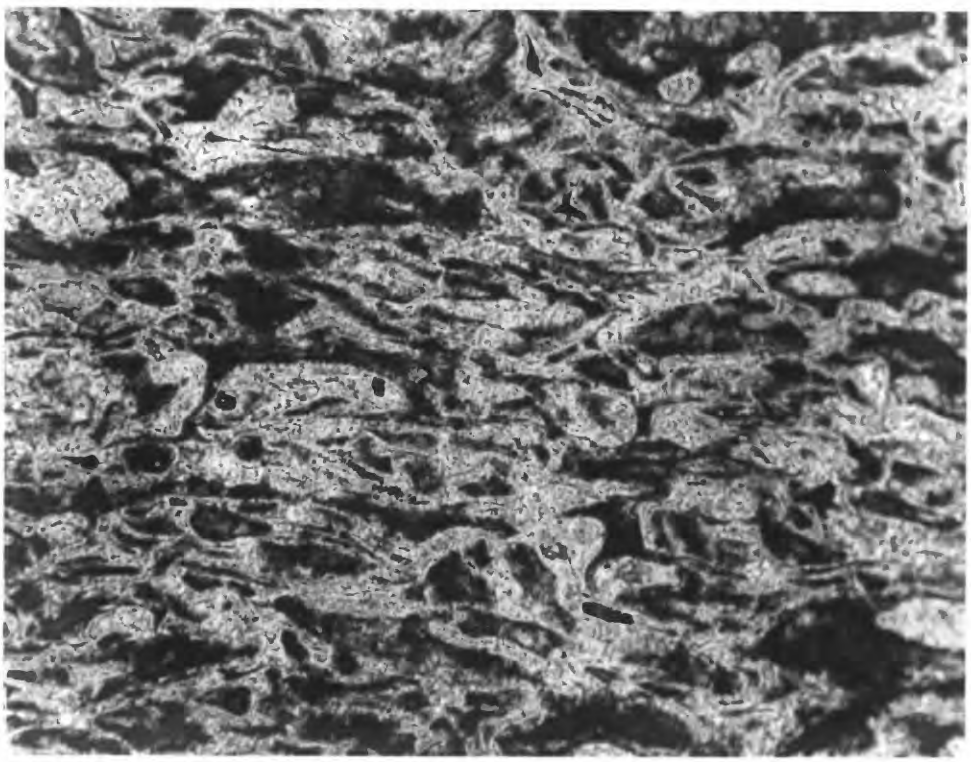

Figure 7.--Photomicrograph of the densely welded base of the lower cooling unit of the Joe Lott Tuff Member. Glass shards are flattened parallel to the plane of compaction. Field of view is 1.8 by 1.4 mm.

Thin section description of the samples studied.

Sample	Description
Crystal-rich tuff member, vitrophyre	Glassy groundmass with minor amounts of pumice fragments, contains ubiquitous euhedral and subhedral phenocrysts of quartz, some embayed, ranging from 3.6 mm to 0.1 mm. Euhedral and subhedral sanidine with some embayed grains are 0.04 to 3.4 mm. Andesine averages 0.4 mm. Yellowish-brown to dark-brown biotite plates average 0.4 mm, but up to 2.2 mm in length. Light-green subhedral augite often with opaque inclusions averages 0.4 mm. Minor rhyolitic lithic fragments with some opaques and iron-oxides.
Joe Lott Tuff Member	
Upper unit	Poorly welded, devitrified groundmass of glass shards and large spherulitically devitrified pumice fragments. Axiolitic structure on devitrified rims of lithophysal cavities, some with vapor-phase crystals. Minor quartz averages 0.5 mm, anorthoclase 0.18 mm, and oligoclase 0.4 mm. Lithic fragments average 0.18 mm but are occasionally up to 2.6 mm.
Pink unit	Glassy groundmass consists of dense concentration of poorly welded, large, broken glass shards. Quartz phenocrysts average 0.5 mm. Elongated tubular pore spaces give fibrous structure to 1.5 mm pumice fragments, some are devitrified. Lithics occasionally iron stained, average 0.4 mm, occasionally 3.2 mm.
Middle unit - top	Poorly welded, devitrified groundmass of glass shards and devitrified pumice. Axiolitic structure on devitrified rims of lithophysal cavities, some with vapor-phase crystals. Some remobilized silica found with devitrification products. Quartz phenocrysts average 0.5 mm and zircon 0.06 mm. Lithics generally 0.3 mm, often iron stained and containing many opaques.
Middle unit - bottom	Poorly welded, devitrified groundmass with some glass shards retaining partial spherical shape. Spherulitically devitrified pumice fragments common. Iron-stained border common on shards. Quartz phenocrysts average 0.6 mm and oligoclase 0.2 mm. Moderate number of iron-stained lithics average 0.8 mm, occasionally to 4.4 mm.
Lower unit - top	Poorly welded, devitrified groundmass of glass shards and spherulitically devitrified pumice. Quartz phenocrysts range from 0.3 to 0.6 mm and sanidine phenocrysts are of similar size. Lithics average 0.4 mm; some are iron-stained and up to 5 mm.
Lower unit - middle	Moderately welded, devitrified groundmass with minor amounts of spherulitically devitrified pumice. Quartz phenocrysts average 0.3 mm and sanidine 0.22 mm. Oligoclase is 0.1 mm. Iron-stained lithics range from 1.4 to 3 mm.

Lower unit - bottom	Densely welded, devitrified groundmass with glass shards flattened parallel to plane of compaction and few spherulitically devitrified pumice fragments. Sanidine phenocrysts average 0.4 mm and oligoclase 0.2 mm. Moderate number of lithics range from 0.3 to 0.8 mm.
Basal vitrophyre	Glassy groundmass of broken shards with perlitic cracks, and devitrified, compressed lithophysae. Quartz phenocrysts average 0.1 mm and sanidine 0.2 mm. Very minor apatite is 0.3 mm. Moderate number of lithics average 0.8 mm, occasionally 8 mm; a few are from the Bullion Canyon Volcanics.

WHOLE-ROCK CHEMISTRY

Whole-rock chemical analyses and CIPW norms of samples from the Joe Lott Tuff Member and the basal vitrophyre of the crystal-rich tuff member are listed in table 4. The major elements in the Joe Lott Tuff Member samples were analyzed by X-ray fluorescence and minor elements by delayed neutron activation and induction coupled plasma optical emission spectroscopy. The major elements in the crystal-rich tuff member were determined by classical wet chemical methods, and supplemental analyses were done by semiquantitative 6-step spectrographic analysis and delayed neutron activation. Loss on ignition (LOI), H_2O^+, and H_2O^- were determined on all samples with the exception of the basal vitrophyre of the crystal-rich tuff member, for which only total H_2O is given. The normative minerals were calculated from the data with a revised version of the graphic normative analysis program (Stuckless and Van Trump, 1979).

The overall chemical homogeneity of the Joe Lott Tuff Member samples is evident in table 4. Most of the iron is present as Fe^{3+}. The tuff has a high alkali content, with a mean value of 8.72 weight percent; K_2O is somewhat higher than Na_2O. This alkali content is about 3 weight percent higher than that of average rhyolites (Washington, 1917), indicating that the Joe Lott Tuff Member crystal-rich tuff member samples are alkali rhyolites. Agpaitic indices [molar $(Na_2O+K_2O)/Al_2O_3$] for the samples, listed in table 5, are all less than one; therefore the rocks are not peralkaline.

The significance of alkali analyses of ash-flow tuffs has been disputed because of subsolidus mobility of alkalis as a tuff cools and secondary devitrification (Lipman, 1965). Several observations do not support major amounts of redistribution of the alkalies and argue for the significance of the reported analyses: (1) All the samples collected are fresh and apparently have undergone no obvious hydrothermal alteration; (2) There is a general consistency of the analyses and a systematic progression is seen in the concentrations with stratigraphy; and (3) There is agreement between the bulk rock chemistry and the coexisting phenocryst compositions (shown in chapter 5).

Table 4.--Whole-rock chemical analyses normalized volatile-free and CIPW norms of the Joe Lott Tuff Member and the crystal-rich tuff member

[D.I., differentiation index; leaders (---), not analyzed for. Analysts for samples M820, M827-M833: X-ray fluorescence by J. S. Wahlberg, J. Baker, and J. Taggart; delayed neutron activation by R. Bies, H. T. Millard, Jr., B. Keaten, M. Coughlin, and S. Lasater; induction coupled plasma optical emission spectroscopy by H. Heiman, F. E. Lichte, F. Newman, and G. Mason. Analysts for sample M672: wet chemical analysis by J. Reid; semiquantitative 6-step spectrographic analysis by M. J. Malcolm; delayed neutron activation by H. T. Millard, Jr., M. Coughlin, B. Vaughn, M. Schneider, and W. Stang. Data in weight percent except as noted]

Sample number---	M820	M827	M828	M829	M830	M831	M832	M833	M672
Lab number-----	D-228264	D-228268	D-228269	D-228270	D-228271	D-228272	D-228273	D-228274	D-215889
SiO_2	75.85	76.64	76.02	77.31	76.65	76.56	76.57	76.11	71.44
Al_2O_3	13.21	12.57	12.53	12.26	12.76	12.90	13.31	12.77	14.72
Fe_2O_3	.87	.91	.98	.92	.78	.93	.84	.91	1.24
FeO	.26	.01	.01	.01	.09	.01	.11	.09	.58
MgO	.21	.20	.31	.42	.21	.20	.60	.20	.36
CaO	.80	.40	.99	.59	.36	.34	.75	.35	1.14
Na_2O	3.80	3.85	3.86	2.81	3.50	3.76	3.51	4.22	4.98
K_2O	4.77	5.15	5.10	5.57	5.49	5.12	4.12	5.15	4.98
TiO_2	.15	.11	.13	.11	.11	.12	.12	.13	.36
P_2O_5	<.1	.10	<.1	<.1	<.1	<.1	<.1	<.1	.07
MnO	.07	.05	.06	<.02	.05	.06	.07	.06	.11
LOI	4.05	1.14	3.59	3.02	1.49	.78	5.42	1.06	---
H_2O^+	2.82	.34	1.49	.91	.90	.39	3.41	.23	2.5
H_2O^-	.68	.33	.86	1.02	.49	.20	1.49	.10	.36
CO_2	.01	<.01	<.01	<.01	<.01	.04	.01	.01	.18
F	.11	.03	.03	.15	.03	.03	.14	.04	.12
Cl	---	---	---	---	---	---	---	---	.03
S	<.01	<.01	<.01	<.01	<.01	<.01	<.01	.02	---
Th-Sn in ppm									
Th	48.3	43.7	39.8	45.0	42.0	43.9	46.7	43.3	25.9
U	13.1	9.67	8.69	6.55	9.34	10.1	11.7	8.91	9.69
Be	6	6	7	5	6	6	6	6	7
Li	40	36	40	20	38	50	39	40	---
Mo	7	4	4	2	3	4	9	<2	5
Nb	48	42	42	41	44	43	45	44	30
Sn	11	<10	<10	20	<10	<10	<10	<10	---
Normative minerals (weight percent, calculated without H_2O and CO_2)									
Q	33.42	33.66	32.13	37.79	34.20	34.10	37.87	31.02	21.11
C	.32	.18		.54	.40	.57	1.71		
OR	28.22	30.43	30.11	32.91	32.47	30.24	24.36	30.42	29.41
AB	32.18	32.60	32.70	23.74	29.60	31.79	29.74	35.73	42.12
AN	3.98	1.30	1.80	2.94	1.79	1.66	3.70	.68	3.14
WO			1.24					.44	.86
EN	.53	.51	.78	1.04	.51	.51	1.49	.50	.90
MT	.66				.14		.25	.11	1.19
HM	.41	.91	.98	.93	.69	.93	.67	.84	.42
IL	.28	.13	.16	.02	.22	.15	.22	.25	.69
IN			.11						
RU		.04		.10		.04			
AP		.24							.17
Total	100.00	100.01	100.00	100.00	100.00	100.00	100.00	100.00	100.01
Salic	98.12	98.18	96.74	97.92	98.45	98.37	97.38	97.86	95.77
Femic	1.88	1.83	3.27	2.09	1.55	1.63	2.63	2.14	4.24
D.I.	93.82	96.69	94.94	94.44	96.26	96.14	91.96	97.18	92.64

Table 5.--Agpaitic indices [molar $(Na_2O+K_2O)/Al_2O_3$] of the Joe Lott Tuff Member and the crystal-rich tuff member

Sample	Description	Index
M672	Vitrophyre-crystal-rich tuff member	0.922
	Joe Lott Tuff Member	
M833	Upper unit	0.980
M832	Pink unit	0.769
M831	Middle unit - top	0.909
M830	Middle unit - bottom	0.917
M829	Lower unit - top	0.868
M828	Lower unit - middle	0.947
M827	Lower unit - bottom	0.948
M820	Vitrophyre	0.865

Selected major and minor elemental concentrations (only those which show variations) from the whole-rock chemical analyses are plotted against stratigraphy in figure 8. Overall trends from the basal vitrophyre to the top of the lower cooling unit include a slight increase in Si and K, and a small decrease in Al, Na, Th, U, Li, Mo, and Nb. The variation in F concentration is erratic. Only minor change is seen in the elemental concentrations above the lower unit; however, the pink unit does differ slightly from the other units, with a somewhat higher F content and a lower K concentration. The crystal-rich tuff member contains less Sr, Th, Nb, and slightly more Fe, Al, and Ca than does the Joe Lott Tuff Member.

In light of analytical uncertainty, meaningful trends in the major elements are only seen in the slight increase in the Si and K content upward in the lower cooling unit. The minor elements, however, exhibit stronger gradients; Th, U, Li, Mo, and Nb all decrease upward in the lower unit. The overall decrease in U, Li, Mo, and Nb is broken by a slight increase between the bottom and middle of the lower unit. This alternation suggests some type of discontinuity not reflected by a separation of cooling units, but significant and discussed later.

Enrichment factors, concentrations in the earliest erupted or roof-zone samples divided by concentrations in deeper derived samples later in the eruptive sequence, are diagrammed in figure 9 and compared with Hildreth's (1981) data for the Bishop Tuff. They are calculated from the whole-rock data (table 4) and neutron activation analyses (table 6) for the basal vitrophyre to the top of lower cooling unit which, by the uniform welding of the cooling unit, represents one fairly continuous eruptive event. The general pattern of overall enrichment and depletion of the Joe Lott Tuff Member is comparable to the Bishop Tuff trend, but disparity exists in the behavior of Ca, Ti, Fe, Co, Sb, and in the LREE La, Ce, Nd, and Eu. Immediately apparent in the Joe Lott Tuff Member is the marked enrichment of Cs which is accompanied by the enrichment (in decreasing intensity) of Li, Na, Ca, Be, and Rb. The depletion of K is antithetic to Na. Water is strongly enriched. First transition series metals Co, Cr, Sc, Ti, and Fe are all enriched--Co to the largest extent. Of the multi-valent cations, Mo exhibits the greatest enrichment followed by U and Nb; Sb is depleted, as is Ta to a lesser degree. Th shows a very slight enrichment, as does Hf, while Zr is mildly depleted. The rare-earth elements (REE) show a gradual increase in enrichment from La through Tb, followed by a decrease to Lu which is slightly depleted.

The concentration of normative minerals Q, Or, and Ab is plotted versus stratigraphy in figure 10. The Q and Or content increase upward in the lower cooling units, in the repetitive fashion. As the decrease in Ab content at the top of the lower cooling unit is not reflected in the feldspar microprobe data, it probably indicates some post-emplacement remobilization of Na.

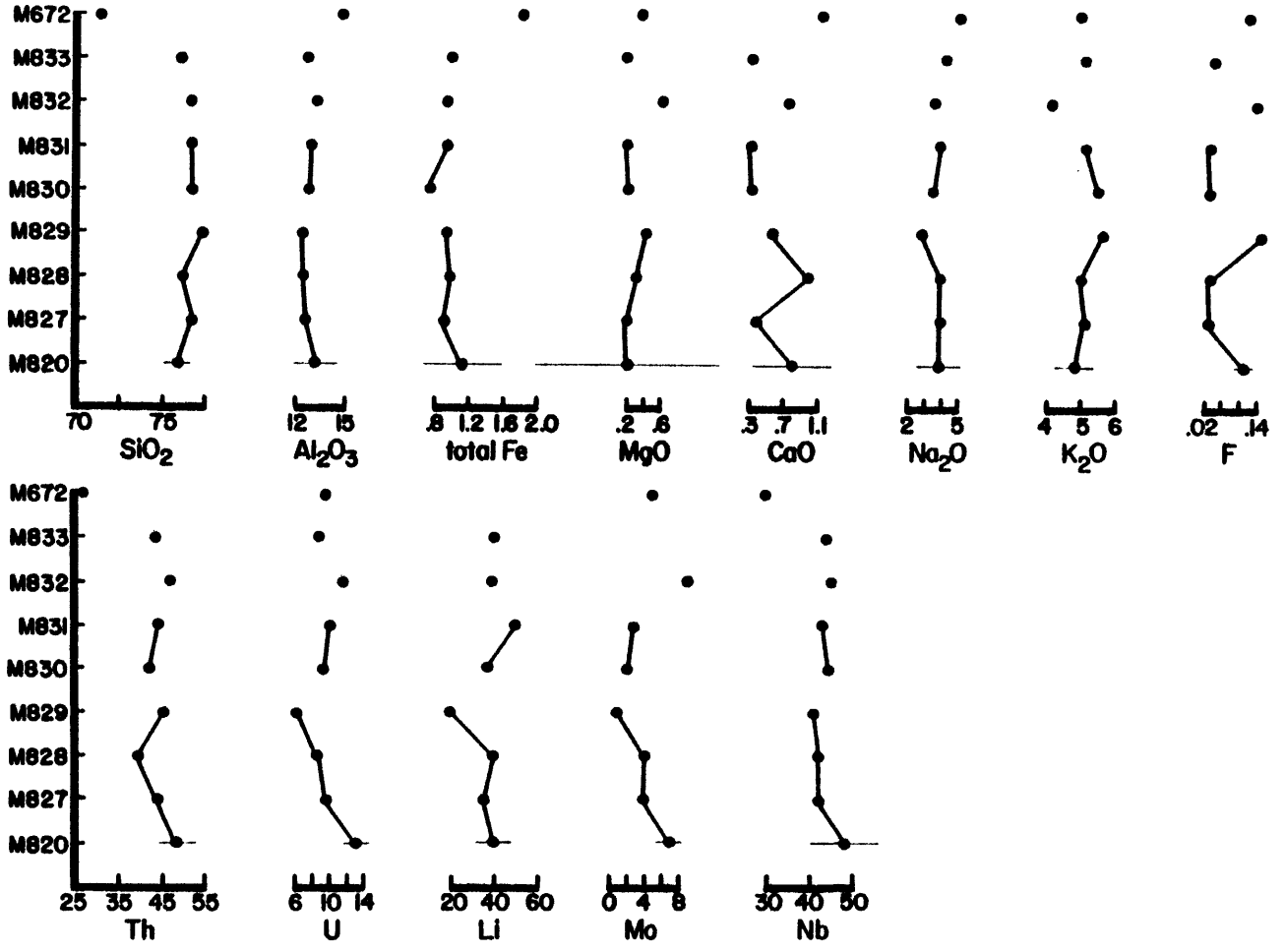

Figure 8.--Variation in whole-rock chemical analyses of the Joe Lott Tuff Member and the crystal-rich tuff member of major elements (normalized, without H_2O) and minor elements with stratigraphy. Concentration in weight percent, with the exception of Th, U, Li, Mo, and Nb in ppm. Total Fe as Fe_2O_3. Mo below detection limit in sample M833. Error bars show analytical uncertainty.

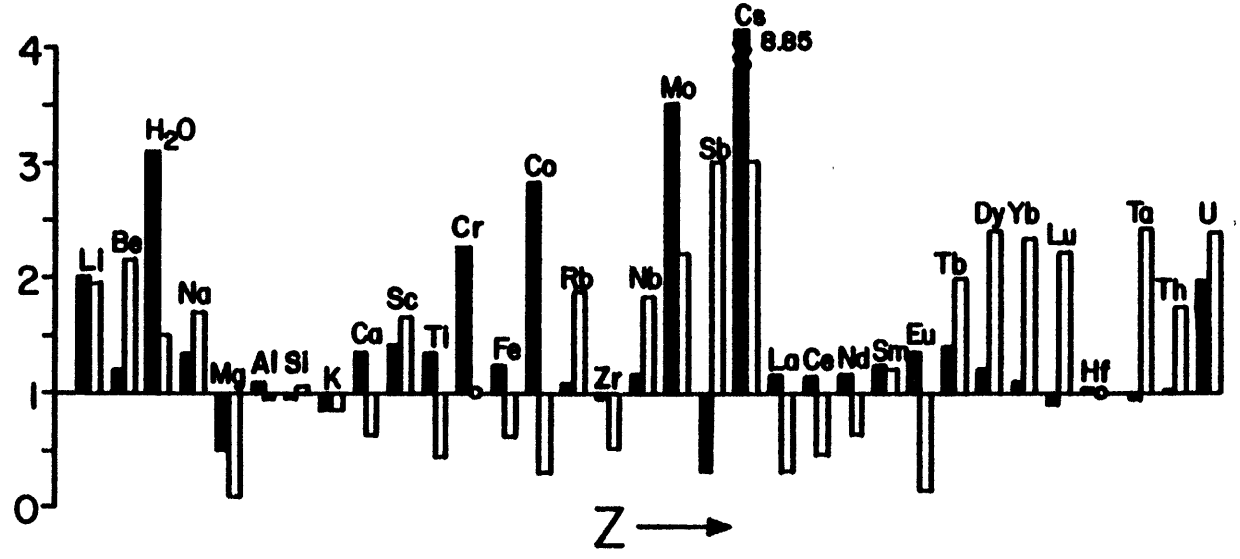

Figure 9.--Enrichment factors (early concentrations/late concentrations) derived from whole-rock data where available for both the Joe Lott Tuff Member (black), data from table 4 and table 6, and the Bishop Tuff (clear), data from Hildreth, 1981.

Table 6.--Instrumental neutron activation analyses, in ppm for the basal vitrophyre (M820) and the top of the lower cooling unit (M829) of the Joe Lott Tuff Member

[Only those values used in the calculation of whole-rock enrichment factors (fig. 10) are listed. Coefficient of variation--C.V.--(±) in ppm. Analysts: J. Budahn and R. Knight]

	M820	C.V.	M829	C.V.
Co	0.837	.025	0.297	.006
Cr	2.89	.06	1.26	.18
Cs	19.2	1.34	2.17	.15
Hf	5.47	.05	5.42	.05
Rb	289	2.89	267	2.67
Sb	.563	.01	1.84	.02
Ta	3.18	.03	3.29	.03
Th	35.8	.36	35.3	.35
U	12.0	.36	6.05	.06
Zr	130	2.60	135	2.70
Sc	2.09	.02	1.47	.01
La	41.9	.42	35.9	.36
Ce	67.5	.68	58.6	1.17
Nd	18.9	.38	16.3	.49
Sm	3.02	.03	2.44	.02
Eu	.284	.006	.208	.002
Tb	.406	.004	.289	.009
Dy	2.76	.11	2.28	.05
Yb	2.22	.02	2.03	.02
Lu	.310	.003	.340	.014

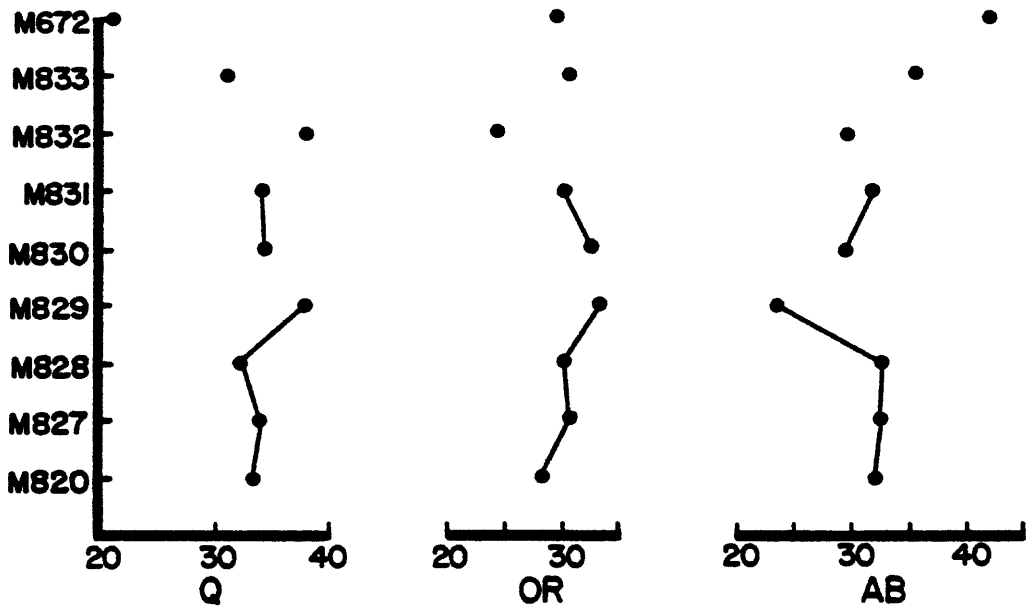

Figure 10.--Variation of normative minerals Q, OR, and AB, in weight percent, with stratigraphy in the Joe Lott Tuff Member and the crystal-rich tuff member.

MINERALOGY AND MINERAL CHEMISTRY

The compositions of phenocrysts in the Joe Lott Tuff Member and the crystal-rich tuff member were studied by analyzing phenocryst separates and polished sections in the electron microprobe. Quartz is the most abundant phenocryst in the Joe Lott Tuff Member; sanidine and oligoclase follow in abundance. Iron and titanium oxide minerals were separated, but only hematite was found in the samples. Biotite, usually oxidized, and augite are found in roughly equal amounts in each of the samples. Apatite, zircon, and sphene occur in the stated order of abundance. The basal vitrophyre of the Joe Lott Tuff Member contains sparse amounts of allanite, chevkinite, hornblende, and fluorite. The fluorite may be secondary.

The crystal-rich tuff member contains approximately 22 percent phenocrysts including, in decreasing abundance, quartz, sanidine, biotite, secondary hematite, augite, andesine, sphene, zircon, and apatite. Table 7 lists the percentages of the various minerals found in the mineral separates made from the Joe Lott Tuff Member and crystal-rich tuff member samples, with the exclusion of quartz and feldspar. The values were obtained by estimating the relative amounts of each mineral in the various separations. These values do not represent absolute modal abundance but may reflect relative abundance between samples, since the separations were performed in a consistent manner.

Sample preparation for microprobe analyses

Feldspar, zircon, apatite, allanite, chevkinite, amphibole, and pyroxene were analyzed by microprobe. They were separated from the samples as follows.

Samples M827-M833 and M820 were crushed and lithic fragments removed by hand. The clean samples were then pulverized, and fed across a Wilfley table in order to float off the large amount (about 99 percent) of glass in the samples. The heavy fractions concentrated on the Wilfley table were then separated by the heavy liquids bromoform and methylene iodide. The splits obtained were separated further magnetically. Sample M672, collected at an earlier date, was crushed, pulverized, and sieved. The less-than-60 mesh but larger-than-120 mesh portion was washed and then put into dilute bromoform, bromoform, methylene iodide, and the magnetic separator.

The minerals to be analyzed by microprobe were mounted in holes in aluminum or brass discs, filled with epoxy, and polished.

Microprobe analyses were done on the U.S. Geological Survey Denver ARLSEMQ microprobe. Electron beam size was approximately 1μ in diameter. Background contributions were measured on either side of the peaks and then averaged. Detection limits for each element of low concentration were calculated at 3σ counts above background.

Table 7.--Mineral percentages, excluding quartz and feldspar, of phenocrysts in the Joe Lott Tuff Member and the crystal-rich tuff member, estimated from the mineral separates

[Leaders (---), none. Note difference between these abundances and modal analyses in table 3]

Sample	Hematite	Pyroxene	Biotite	Sphene	Apatite	Zircon	Allanite/ Chevkinite	Fluorite
Crystal-rich tuff member,								
vitrophyre----------	28		17	52	2	0.1	0.6	------
Joe Lott Tuff Member								
Upper unit----------	57		8	11	0.4	1	0.6	------
Pink unit----------	73		15	7	2	2	1	------
Middle unit - top----	97		2	---	0.1	0.2	1	------
Middle unit - bottom-	50		14	18	0.2	18	0.5	------
Lower unit - top-----	93		3	2	0.2	0.2	2	------
Lower unit - middle--	90		0.1	8	---	1	1	------
Lower unit - bottom--	86		4	6	0.3	3	1	------
Vitrophyre----------	88		6	0.7	0.7	2.5	1.2	0.50.3

Microprobe operating conditions were set up as follows:

Mineral analyzed	Accelerating voltage	Current	Data reduction method
Feldspar	10 kv	10 nanoamps on brass	Bence-Albee
Zircon	20 kv	10 nanoamps on brass	MAGIC
Apatite	15 kv	10 nanoamps on brass	MAGIC
Allanite	15 kv	10 nanoamps on brass	MAGIC
Chevkinite	15 kv	10 nanoamps on brass	MAGIC
Amphibole	15 kv	10 nanoamps on brass	Bence-Albee
Pyroxene	15 kv	10 nanoamps on brass	Bence-Albee

The following standards were used:

Mineral analyzed	Standards
Feldspar	Amelia albite (Na), Clear Lake plagioclase (Si, Al, Ca), Benson orthoclase (K)
Zircon	Ceylon zircon (Si, Zr, Hf), euxenite (U), Durango apatite (P, La), REE standard 3 (Drake and Weill, 1972)--(Y, Ce, Pr)
Apatite	Durango apatite (F, P, Ca), Lemhi biotite (Cl), fayalite (Mn), USGS synthetic glass (Mg), REE standard 2 (Nd), REE standard 3 (Pr, Ce, Y, La)
Allanite and Chevkinite	dolomite (Mg), Wilberforce apatite (F, Na), Peerless apatite (P, Mn), biotite (Fe), sphene (Ca, Ti), REE standard 2 (Nd, Sm), REE standard 3 (Al, Y, La, Ce, Pr), Ceylon zircon (Si), ThO_2 pure (Th), uraninite (U)
Amphibole and Pyroxene	USGS synthetic glass (Na, Al, Fe, K, Ca), orthopyroxene (Si, Mg, Mn, Ti, Cr)

Feldspar

Plagioclase and particularly potassium feldspar are quite common in all samples. Clear to white euhedral grains range in size from 170 to 240μ in length. Core and rim compositions were determined on randomly selected feldspar separates from each sample. The results for each sample were averaged. Little variation in core vs. rim composition was observed with the exception of potassium feldspar jackets on some plagioclase grains in samples M827 and M831. An, Ab, and Or were calculated from CaO, Na_2O, and K_2O.

To insure that feldspars from xenocrysts were not being analyzed in the mineral separates, feldspars were also probed in polished thin sections. All the crystals present in the slides were probed; however, when sample concentration was great enough, analysis was stopped when a representative sampling was obtained. Good correlation exists between the two sets of data, and similar trends are observed.

Compositions of the potassium feldspar and the plagioclase for both the mineral separates and the thin sections are given in tables 8 and 9. Relative abundance of the two minerals, per sample, is also listed. As the compositional data for the mineral separates and the thin sections closely parallel each other only the mineral separate data will be discussed and diagrammed from this point on. Plagioclase was observed in some thin sections but not in the corresponding mineral separates. The reason for this is not clear. The data on the mineral separates are representative of a much larger sample population, whereas the thin section data are obtained from only one or two polished thin sections.

Table 8.--Microprobe analyses of representative feldspar separates in the Joe Lott Tuff Member and the crystal-rich tuff member

[Analyses in weight percent]

Sample	Description	Potassium feldspar				Plagioclase			
		Proportion (in %)	An	Ab	Or	Proportion (in %)	An	Ab	Or
M672	Crystal-rich tuff member, vitrophyre--	85	4.43	57.50	38.08	15	35.80	59.30	4.90
	Joe Lott Tuff Member								
M833	Upper unit----------	100	3.25	63.52	33.29				
M832	Pink unit----------	100	2.72	62.96	34.32				
M831	Middle unit - top----------	93	2.78	56.66	40.58	7	29.25	66.93	3.82
M830	Middle unit - bottom----------	100	.75	40.96	58.29				
M829	Lower unit - top----------	50	2.28	44.06	53.67	50	24.92	71.77	3.32
M828	Lower unit - middle----------	60	.98	37.14	61.89	40	20.33	75.24	4.44
M827	Lower unit - bottom----------	93	3.65	57.00	39.35	7	11.78	81.29	6.93
M820	Vitrophyre----------	100	.73	38.49	60.78				

Table 9.--Microprobe analyses of representative feldspar in thin sections of the Joe Lott Tuff Member and the crystal-rich tuff member

[Analyses in weight percent]

Sample	Description	Potassium feldspar				Plagioclase			
		Proportion (in %)	An	Ab	Or	Proportion (in %)	An	Ab	Or
M672	Crystal-rich tuff member, vitrophyre--	88	3.13	53.51	43.36	12	29.56	65.18	5.26
	Joe Lott Tuff Member								
M833	Upper unit----------	100	2.93	62.95	34.13				
M832	Pink unit----------	57	1.87	45.18	52.95	43	24.52	70.08	5.41
M831	Middle unit - top----------	67	1.49	43.72	54.80	33	24.75	69.61	5.66
M830	Middle unit - bottom----------	50	0.66	39.74	59.60	50	19.38	74.75	5.88
M829	Lower unit - top----------	43	1.34	44.17	54.50	57	17.69	73.99	8.33
M828	Lower unit - middle----------	78	0.92	39.91	59.17	22	11.59	82.24	6.17
M827	Lower unit - bottom----------	71	2.91	53.38	43.72	29	19.83	74.70	5.47
M820	Vitrophyre----------	33	1.03	51.50	47.49	67	22.95	72.56	4.49

The ternary diagram in figure 11 defines the feldspars as sanidine and oligoclase (Deer and others, 1963). The plagioclase in the crystal-rich tuff member is an andesine. Throughout the eruptive history of the Joe Lott Tuff Member, the sanidine becomes more sodic--increasing from 38.49 weight percent Ab in the lower unit to 63.52 weight percent Ab in the upper unit. In this same interval, Or drops from 60.78 to 33.29 weight percent and An increases slightly from 0.73 to 3.25 weight percent. The sodic concentration of the sanidine increases in three separate cycles (table 8):

(1) basal vitrophyre through bottom of lower cooling unit,
(2) middle to top of lower cooling unit, and
(3) bottom of middle through upper cooling unit.

During the eruptive history of the Joe Lott Tuff Member, the plagioclase systematically becomes more calcic (fig. 11). From the lower unit to the top of the middle unit, An increases from 11.78 to 29.25 weight percent, Ab drops from 81.29 to 66.93 weight percent and Or decreases slightly from 6.93 to 3.82 weight percent.

A plot of the weight percent Or, weight percent Ab, and weight percent An in the sanidine against stratigraphy (fig. 12) more clearly illustrates the trends seen in the ternary diagram (fig. 11). Moving up in the section the Or content decreases, the Ab content increases, and the An content increases slightly. In the upper two units, Or concentration remains at its lowest level and Ab content stays fairly high. This drop in the Or content of the sanidine upward in stratigraphy occurs in the Bandelier Tuff (Smith and Bailey, 1966).

A similar graph for oligoclase composition in plagioclase versus stratigraphy is shown in figure 13. Plagioclase is absent in the feldspar separates from the basal vitrophyre, bottom of the middle unit, pink, and upper units. In both the lower and middle units, the An content increases upward to about 30 weight percent, while the concentration of Ab drops slightly from about 80 to 70 weight percent. The Or content drops slightly in both the lower and middle units. The reequilibration between the lower and middle cooling units is again evident.

The compositions of plagioclase found in the thin section samples but not in the mineral separates (M820, M830, M832) are shown as circles in figure 13. This data illustrates a smoother increase in An content and decrease in Ab content throughout the lower and middle cooling units. The composition of the plagioclase found in the pink unit is fairly close to that of the plagioclase in the top of the middle unit.

The relative abundance of potassium feldspar versus plagioclase is plotted against stratigraphy in figure 14. Sanidine content steadily decreases going upward in the lower cooling unit from 100 to 50 percent. Reequilibration of the magma chamber is again seen by the 100 percent sanidine content in the bottom of the middle unit. The pink and upper units both contain 100 percent sanidine. The basal vitrophyre of the crystal-rich tuff member has 85 percent sanidine. This systematic variation in relative abundance of feldspars has been observed during the progressive eruption of many other large volume silicic magma chambers (Hildreth, 1981).

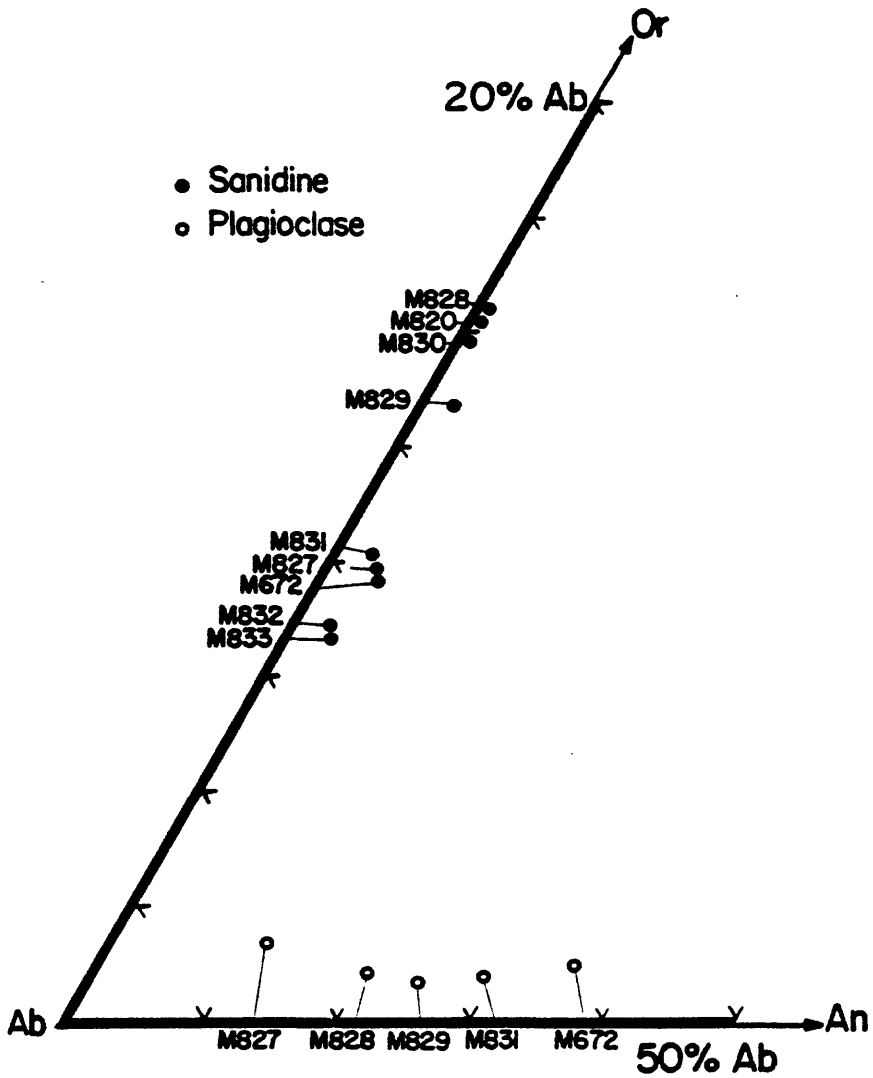

Figure 11.--Ternary plot of feldspar compositions in weight percent Ab, Or, and An in the Joe Lott Tuff Member and the crystal-rich tuff member.

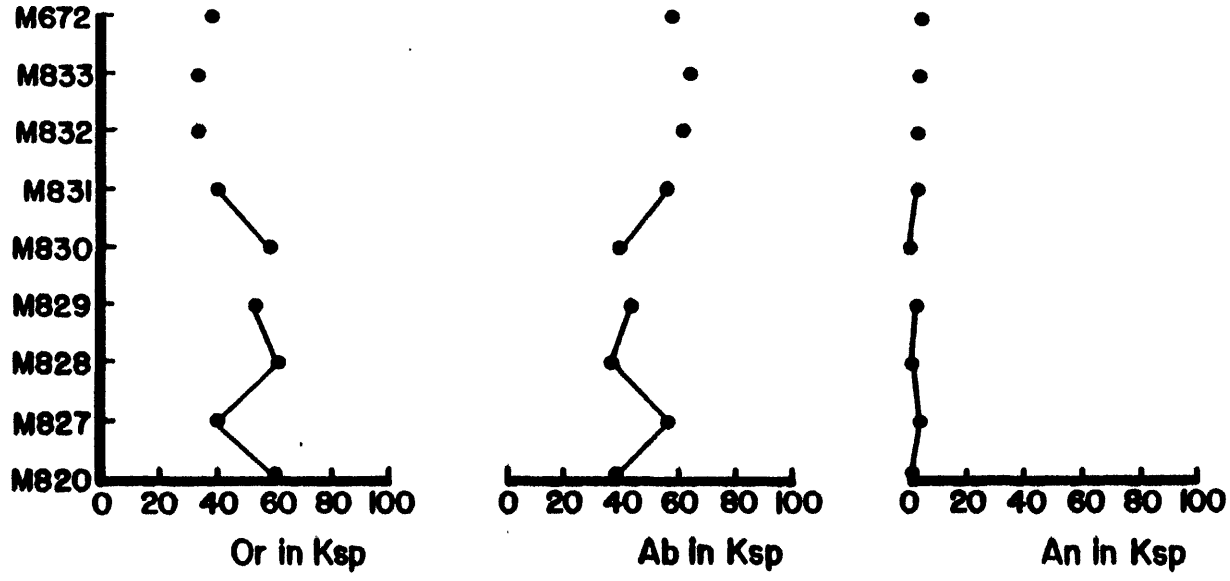

Figure 12.--Variation of weight percent Or, Ab, and An in sanidine with stratigraphy in the Joe Lott Tuff Member and the crystal-rich tuff member.

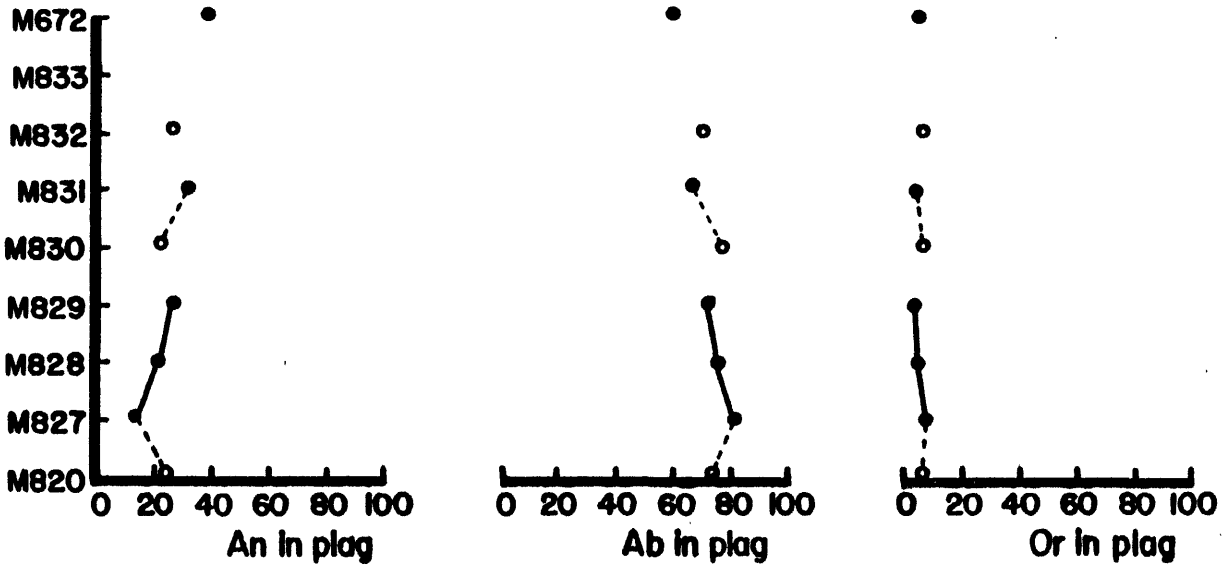

Figure 13.--Variation of weight percent An, Ab, and Or in plagioclase with stratigraphy in the Joe Lott Tuff Member and the crystal-rich tuff member. Thin section data represented by circles.

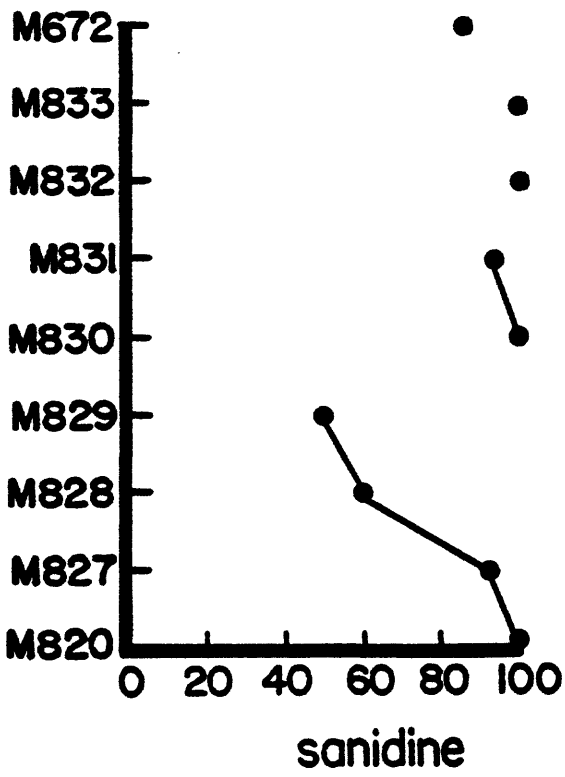

Figure 14.--Variation in relative proportion of sanidine versus feldspar, in percent, with stratigraphy in the Joe Lott Tuff Member and the crystal-rich tuff member.

Crystal-rich tuff member

Some early preliminary X-ray work was done on the alkali feldspar from the crystal-rich tuff member (samples M74 and M75). The 2θ values were used to estimate structural state and composition using the method outlined by Wright (1968). Measured 2θ values are as follows:

	$\bar{2}04$	060
M74	51.13°	41.90°
M75	51.16°	41.93°

Figure 15 relates observed 2θ values to appropriate computed cell parameters of feldspars of known structural states. Equations relating cell dimensions to 2θ values are computed using a standard least-squares program. The measured 2θ values for samples M74 and M75 are plotted in figure 15 and indicate a high or disordered structural state and a composition intermediate between the potassic and sodic end members.

Microprobe analyses of the samples by Alexander Gunow are given below.

	An	Ab	Or
	(in weight percent)		
M74 (average of 4 grains)	2.2	67.3	30.5
M75 (average of 6 grains)	2.2	55.8	42.0

Zircon

Two different populations of zircons are present in each sample: in one case as larger (230 μ long) clear grains and in the other as smaller (110 μ) pink ones. Both types occur as dipyramidal euhedra.

The core and rim of ten grains from both populations in all samples were analyzed by microprobe. Concentrations of ZrO_2, HfO_2, and SiO_2 are homogeneous and were averaged for each sample. Concentrations of UO_2 and the rare-earth elements are variable. Analyses above detection limit are averaged for each sample and, along with the number of meaningful analyses out of the total number of runs, are given in table 10. Concentrations of P_2O_5 and Pr_2O_5 are below calculated detection limits in all samples.

Due to the severe interference problems involved in the analysis of the rare-earth elements, particularly the heavy ones, spectrum stripping on the microprobe was used to determine the REE concentrations. For this procedure, counts were recorded on the peak of each element, its background, and on the interfering element in a standard of known concentration. Peak and background counts for each element were determined on the unknowns. Only one spectrometer was used to insure similar operating conditions during measurement of both the element and its interfering element. After subtracting the contributions of background and the interfering element from the element in question, corrected readings of intensity versus concentration were established to determine weight percent of the unknowns.

Spectrum stripping was used for the REE Nd through Lu in the zircon from the basal vitrophyre. Inasmuch as all concentrations of these elements were found to be below detection limits, this procedure was not attempted on any other sample.

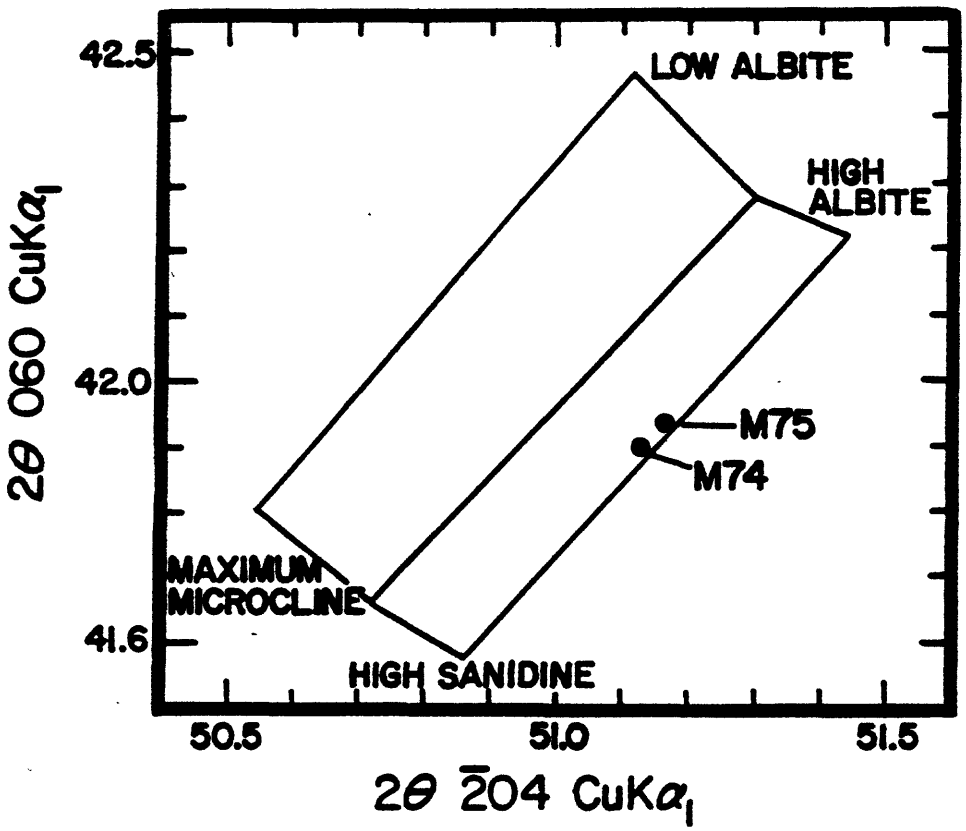

Figure 15.--Feldspar alkali exchange paths and structural states on a plot of 2θ(060) against 2θ($\bar{2}$04). Measured 2θ values of $\bar{2}$04 CuKα_1 and 060 CuKα_1 X-ray diffraction peaks of the crystal-rich tuff member samples are shown.

Table 10.--Representative microprobe analyses of zircon in the Joe Lott Tuff Member and the crystal-rich tuff member

[Analyses given in weight percent. Concentrations of Pr_2O_5 below detection limit (0.14 weight percent) and P_2O_5 below detection limit (0.10 weight percent). Fraction in parentheses indicates number of analyses the element was detected out of total number of analyses. Standard deviation of each oxide for all samples as follows: ZrO_2±0.6, HfO_2±0.1, UO_2±0.02, Y_2O_3±0.25, La_2O_3±0.1, Ce_2O_3±0.03, SiO_2±0.13]

Sample	Description	Population	ZrO_2	HfO_2	UO_2	Y_2O_3	La_2O_3	Ce_2O_3	SiO_2	Total	Zr/Hf
M672	Crystal-rich tuff, vitrophyre------	Pink	65.51	1.08	0.22 $\frac{5}{10}$	1.75 $\frac{2}{10}$	0.30 $\frac{2}{10}$	0.12 $\frac{2}{10}$	32.78	101.76	53.0
		Clear	64.60	1.01	.38 $\frac{4}{6}$	1.63 $\frac{3}{6}$	.34 $\frac{1}{6}$	.14 $\frac{2}{6}$	32.45	100.55	55.8
	Joe Lott Tuff										
M833	Upper unit----------	Pink	65.48	1.24	.17 $\frac{2}{8}$	<.80	<.18	<.05	32.75	99.64	46.1
		Clear	64.50	1.21	.11 $\frac{6}{10}$	.74	<.18	<.05	33.16	99.72	46.5
M832	Pink unit----------	Pink	65.03	1.10	.18 $\frac{6}{12}$	1.75 $\frac{8}{12}$	<.18	.15 $\frac{5}{12}$	33.15	101.36	51.6
		Clear	65.87	1.19	.11 $\frac{6}{10}$	<.60	.23 $\frac{2}{10}$	<.05	33.17	100.57	48.3
M831	Middle unit - top----------	Pink	65.71	1.14	.10 $\frac{1}{10}$	1.35 $\frac{2}{10}$	.23 $\frac{2}{10}$	<.05	32.20	100.73	50.3
		Clear	65.08	1.09	.11 $\frac{6}{10}$	.84 $\frac{1}{10}$	<.18	.09	32.85	100.06	51.3
M830	Middle unit - bottom----------	Pink	65.59	1.20	.19 $\frac{2}{12}$	<.84	.27 $\frac{2}{12}$	.11 $\frac{3}{12}$	32.63	99.99	47.7
		Clear	65.00	1.17	.13 $\frac{8}{10}$	1.12	.36 $\frac{1}{10}$	<.05	33.37	101.15	48.5
M829	Lower unit - top----------	Pink	66.51	1.19	.11 $\frac{3}{11}$	1.54	<.18	.10 $\frac{1}{11}$	33.40	102.85	48.8
		Clear	64.24	1.27	.19 $\frac{8}{10}$	1.21	<.18	<.05	33.17	100.08	44.2
M828	Lower unit - middle----------	Pink	65.78	1.27	.73 $\frac{3}{10}$	1.29	.27 $\frac{1}{10}$	<.05	32.79	102.13	45.2
		Clear	65.98	1.40	.16 $\frac{4}{10}$	.43	<.18	<.05	33.00	100.97	41.2
M827	Lower unit - bottom----------	Pink	66.09	1.24	.59 $\frac{5}{10}$	1.01	<.18	.12 $\frac{1}{10}$	32.93	101.98	46.5
		Clear	65.08	1.17	.11 $\frac{6}{10}$	.90	.27 $\frac{2}{10}$	.09 $\frac{1}{10}$	32.97	100.59	48.6
M820	Vitrophyre----------	Pink	64.80	1.17	.15 $\frac{5}{10}$	1.11	.23 $\frac{1}{10}$	.18 $\frac{1}{10}$	32.51	100.15	48.4
		Clear	65.18	1.02	.14 $\frac{5}{8}$	.73	<.18	<.05	32.90	99.97	55.8

Selected oxide concentrations in the zircons are plotted against stratigraphy in figure 16. Within each sample, the composition of the zircon is homogeneous, with slight variations being erratic and not evident in all the grains analyzed.

There is little variation in composition between the clear and the pink populations of zircons. The pink color has been associated with increased crystal structure damage due to higher uranium concentration or greater age (C. W. Naeser, personal commun., 1982). The pink zircons in the bottom and middle of the lower cooling unit have a higher uranium content.

The Si, Zr, and Hf content of zircons is uniform throughout the eruption of the Joe Lott Tuff Member. The drop in Zr/Hf from the basal vitrophyre through the middle of the lower cooling unit in the clear grains, is due to a slight systematic rise in Hf content. The ratio drops off for both species of zircons moving upward in stratigraphy through the top of the middle cooling unit, reflecting the decreasing Hf content.

The Y content of both the pink and clear populations increases in the lower cooling unit and, moving upward in stratigraphy, remains at this level in the pink grains. Perhaps the crystal structure of the pink zircons which incorporated more U, also allowed the grains to accept more Y. Any indication in the zircon data of any discontinuity in the eruption forming the lower cooling unit, can only be seen by the behavior of Y in the clear zircons.

Microprobe analysis of the REE in the zircons was less successful. Detectable concentrations of La, Ce, and Pr are so low and erratically distributed throughout the stratigraphy that REE behavior is undefined. On the whole, partitioning of these elements appears to favor the pink grains. The average sum of the REE concentration detected, per sample collected, is 0.33 percent by weight (La + Ce).

Enrichment factors calculated where data are available for the basal vitrophyre to the top of the lower cooling unit are shown in figure 17. The Joe Lott Tuff Member shows a strong enrichment upward in Ce and a lesser one for U (pink grains), indicating a higher concentration in early erupted samples. A depletion is seen in Y, Hf, and U (clear grains). The opposite enrichment patterns for U in the pink and clear grains reflects the higher U content of early-erupted pink zircons.

Enrichment factors for the Bishop Tuff (Hildreth, 1977) are shown for comparison. With the exception of Y, Ce, and Hf, the pink zircons tend to show enrichment trends more similar to the Bishop Tuff than the clear zircons.

Only minor variation in composition is seen in the microprobe data on the clear versus the pink population of zircon crystals. The ratios of certain elements, normalized and plotted on a ternary diagram, may show chemical variations more readily. Effinroff (1972) used Th/Zr, Hf/Zr, and Y/Zr to determine the correlation of three zircon crystal habit classes with crystal chemistry.

Figure 18 illustrates the U/Zr, Hf/Zr, and Y/Zr for the pink (larger) and clear (smaller) zircons in the Joe Lott Tuff Member. Two distinct, chemically different groups are seen by the two populations. The clear zircon from the crystal-rich tuff member (M672) falls far from the Joe Lott Tuff Member clear zircon field.

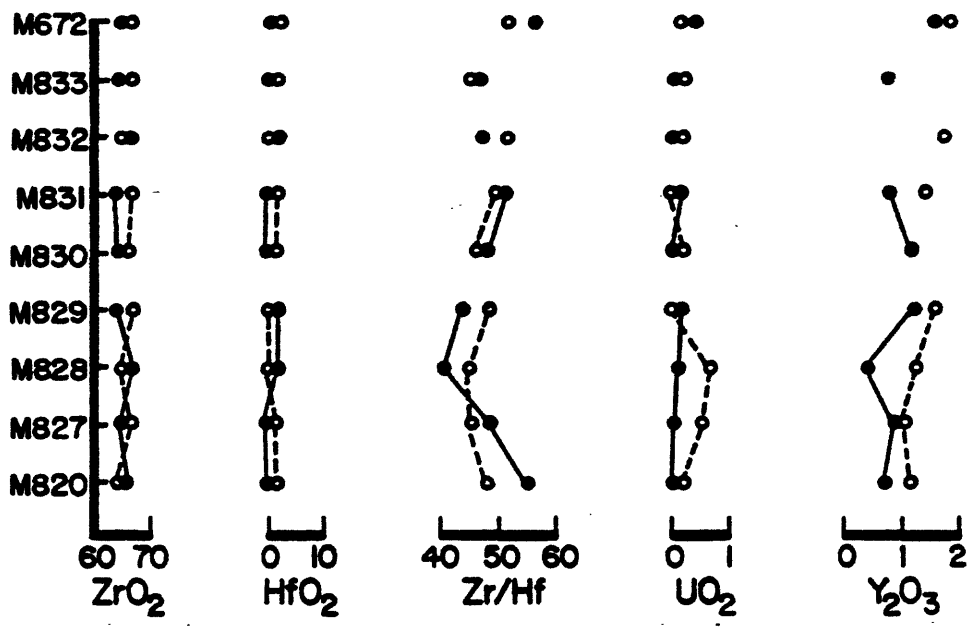

Figure 16.--Variation in clear (.) and pink (o) zircon compositions in weight percent, with stratigraphy in the Joe Lott Tuff Member and the crystal-rich tuff member. Y_2O_3 not detected in all samples.

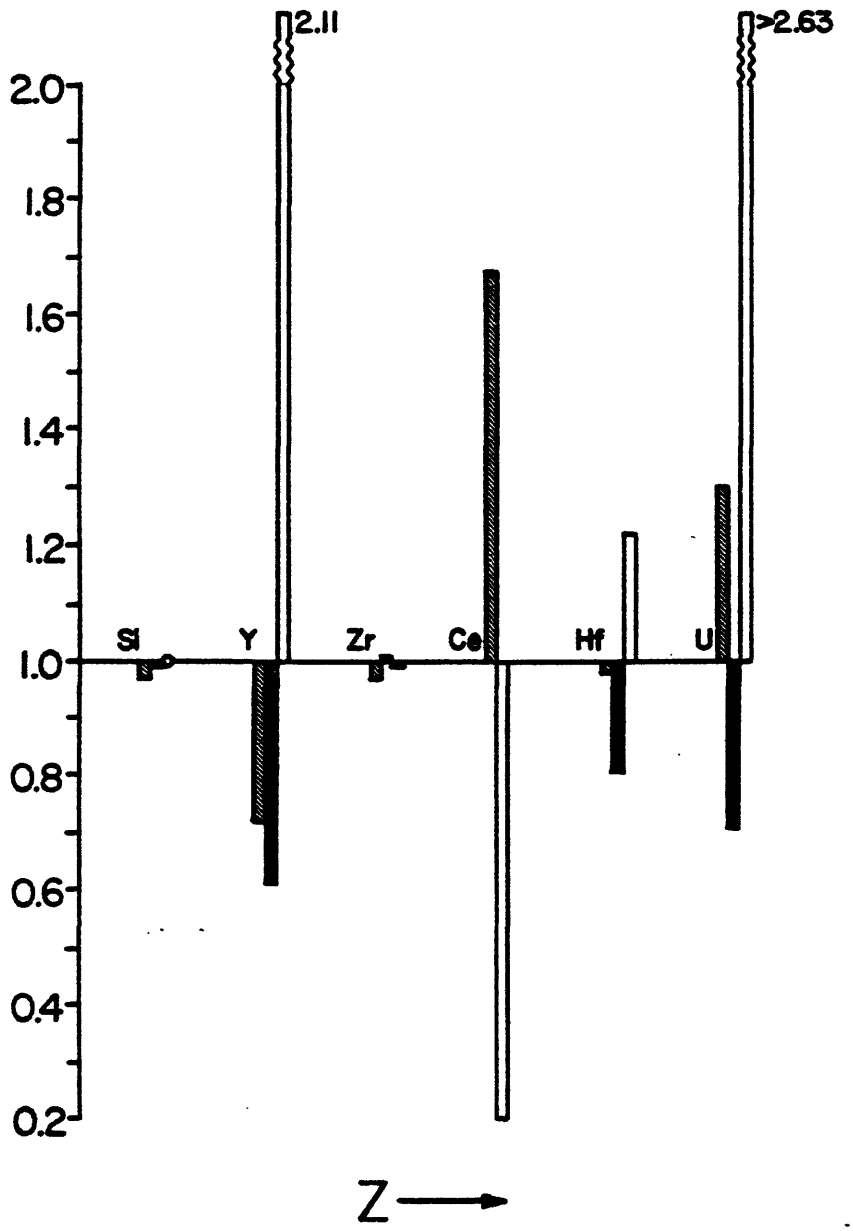

Figure 17.--Enrichment factors (early concentrations/late concentrations) for the Joe Lott Tuff Member clear zircons (black) and pink zircons (diagonal stripe) shown where data are available along with enrichment factors for zircons from the Bishop Tuff (clear) (Hildreth, 1977).

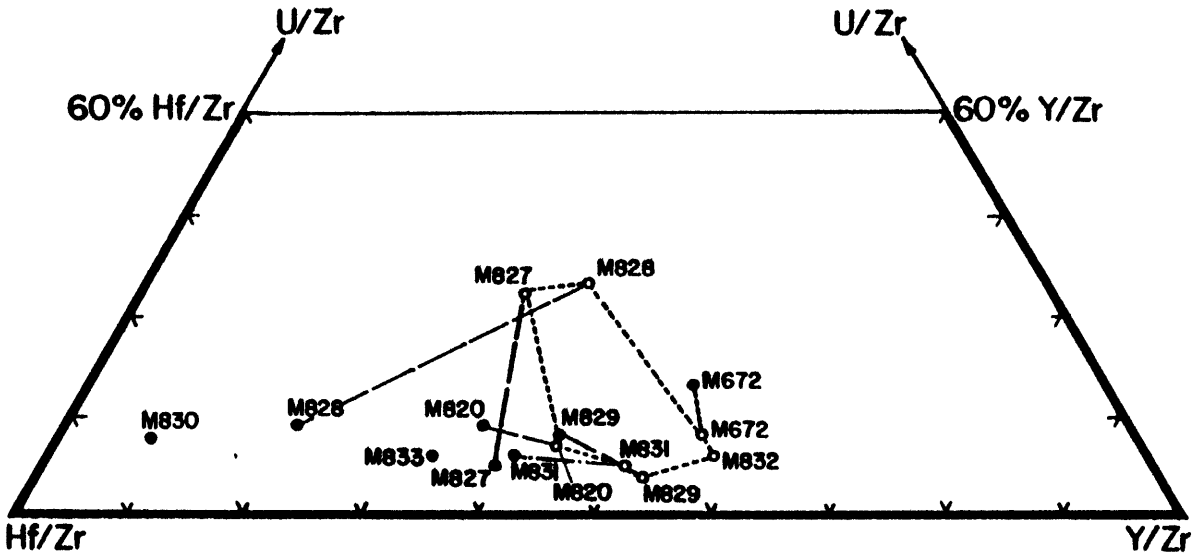

Figure 18.--Ternary plot of normalized U/Zr, Y/Zr, and Hf/Zr content in the clear (.) and pink (o) zircons in the Joe Lott Tuff Member and the crystal-rich tuff member. Tie lines drawn between coexisting clear and pink zircon as follows:

crystal-rich tuff member, vitrophyre - short dashes
Joe Lott Tuff Member
middle cooling unit - dash, dot, dash
lower cooling unit and basal vitrophyre - long dashes

The two groups indicate the distinct chemical difference in the populations. The clear zircon has a higher Hf/Zr content than the other group, while the pink species has a higher Y/Zr content than the other group, while the pink species has a higher Y/Zr concentration. With the exception of the pink zircons of M827 and M828, which are exceptionally high in U, the U/Zr of all the zircons does not vary much. No clear progression in compositional change relative to eruptive history is observed by the tie lines in figure 18.

Apatite

Apatite is found as 140-280 μ long, clear to orange prismatic crystals often terminated by a pyramid and a basal plane. The cores and rims of five grains from each sample were analyzed by microprobe (table 11). Values for Cl, F, Nd_2O_3, Pr_2O_3, Ce_2O_3, La_2O_3, Y_2O_3, MgO, and MnO are not always greater than calculated detection limits. The meaningful values for these elements are averaged and listed along with the total number of analyses made in table 11. The average sum of the REE detected per sample collected is 1.33 percent by weight (La+Ce+Pr+Nd).

Apatite compositions versus stratigraphy are plotted in figure 19. Gradients are established by the majority of the elements throughout the lower cooling unit, and the same trends are often repeated in the middle unit. A discontinuous pattern is evident in the lower cooling unit exemplified to varying degrees by most of the elements detected by the microprobe.

The concentration of P, Nd, Ce, and La all increased upward in the lower cooling unit, whereas Mg decreases. All these elements exhibit discontinuous behavior in their overall trend. Between the lower and middle cooling units, the content of P, Ce, and La all drop and then rise again with the eruption of the middle cooling unit. Nd, Ce, and La all show a small increase between the pink and upper units. Certain elemental concentrations increase as others decrease which is reflected in the enrichment values. This complementary behavior is exhibited by Pr and Ce.

The behavior of Cl, F, Ca, and Mn is not as clear cut; however, a different trend begins after the middle of the lower unit. In three of these cases, the new pattern set at this point is continued throughout the middle cooling unit. Mn, on the other hand, increases in the middle unit after a decrease between the middle and top of the lower unit. These five elemental concentrations remain fairly constant in the upper and pink units, with the exception of Ca which increases slightly.

Enrichment factors where data are available for the basal vitrophyre through the top of the lower cooling unit are shown in figure 20. Markedly strong enrichment is seen in Cl and to a lesser extent in F, Ca, and La. Ce, Mg, and P are depleted. Enrichment factors for the Bishop Tuff (Hildreth, 1977) are shown for comparison, and different patterns exist for Cl and La.

Coexisting zircon is enriched in Ce and U (pink grains) and depleted in Y, La, Hf, and U (clear grains). Data for both minerals are only known for Ce and La. Partitioning of Ce favored zircon, while partitioning of La favored apatite in the early erupted roof-zone samples. The later erupted samples contain more Ce in the apatite and increased La in the zircon.

Table 11.--Representative microprobe analyses of apatite in the Joe Lott Tuff Member and the crystal-rich tuff member

[Analyses given in weight percent. Fraction in parentheses indicates number of analyses the element was detected out of total number of analyses. Standard deviation of each element and oxide for all samples as follows: Cl±0.02, F±0.15, P_2O_5±0.26, CaO±0.13, Nd_2O_3±0.04, Pr_2O_3±0.11, Ce_2O_3±0.08, Y_2O_3±0.03, Le_2O_3±0.03, MgO±0.02, MnO±0.01]

Sample	Description	Cl	F	P_2O_5	CaO	Nd_2O_3	Pr_2O_3	Ce_2O_3	Y_2O_3	La_2O_3	MgO	MnO	Total
M672	Crystal-rich tuff, vitrophyre------	0.17	2.90 9/11	36.53	53.56	0.34	0.35 3/11	0.71	0.15 1/11	0.31 9/11	0.22	0.15	95.39
	Joe Lott Tuff												
M833	Upper unit----------	.11 3/8	3.16	38.37	55.30	.40 6/8	.55 1/8	.62 6/8	.15 3/8	.22	.17	.09 3/8	99.14
M832	Pink unit----------	.32 8/10	3.07	38.53	55.65	.26	<.25	.53	<.06	.20	.15	.09 2/10	98.80
M831	Middle unit - top----------	.15 5/10	3.02	38.65	53.65	.29 9/10	<.25	.51 9/10	<.06	.26 6/10	.31 6/10	.19	97.03
M830	Middle unit - bottom----------	.14 5/10	3.76	38.47	52.84	.31 6/10	<.25	.45 7/10	<.06	.16 8/10	.28 9/10	.13	96.54
M829	Lower unit - top----------	.22 6/10	2.90	39.00	53.02	.24	<.25	.65 9/10	<.06	.23 8/10	.17	.10	96.53
M828	Lower unit - middle----------	.10 6/10	3.40	38.26	52.36	.22	.50 1/10	.56 9/10	.19 1/10	.18 9/10	.23 9/10	.24 8/10	96.24
M827	Lower unit - bottom----------	.12 4/10	3.62	38.06	53.40	.27	.39 2/10	.64 9/10	<.06	.24	.15 9/10	.09 6/10	96.98
M820	Vitrophyre----------	.39 6/10	3.15	37.40	54.61	.24	.50 1/10	.50	<.06	.24 9/10	.16 9/10	<.02	97.19

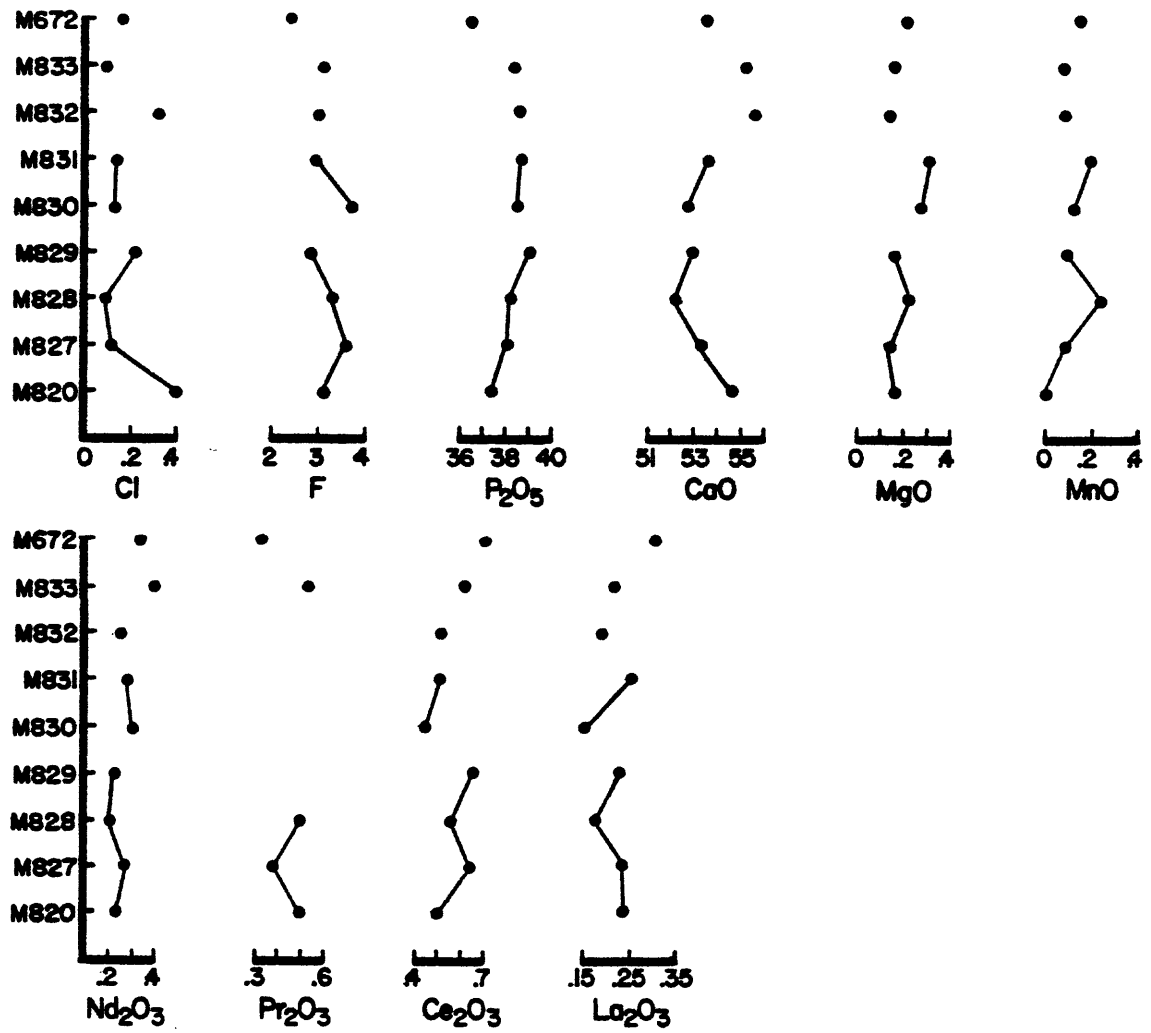

Figure 19.--Variation in apatite composition, in weight percent, with stratigraphy in the Joe Lott Tuff Member and the crystal-rich tuff member. Pr_2O_3 not detected in all samples.

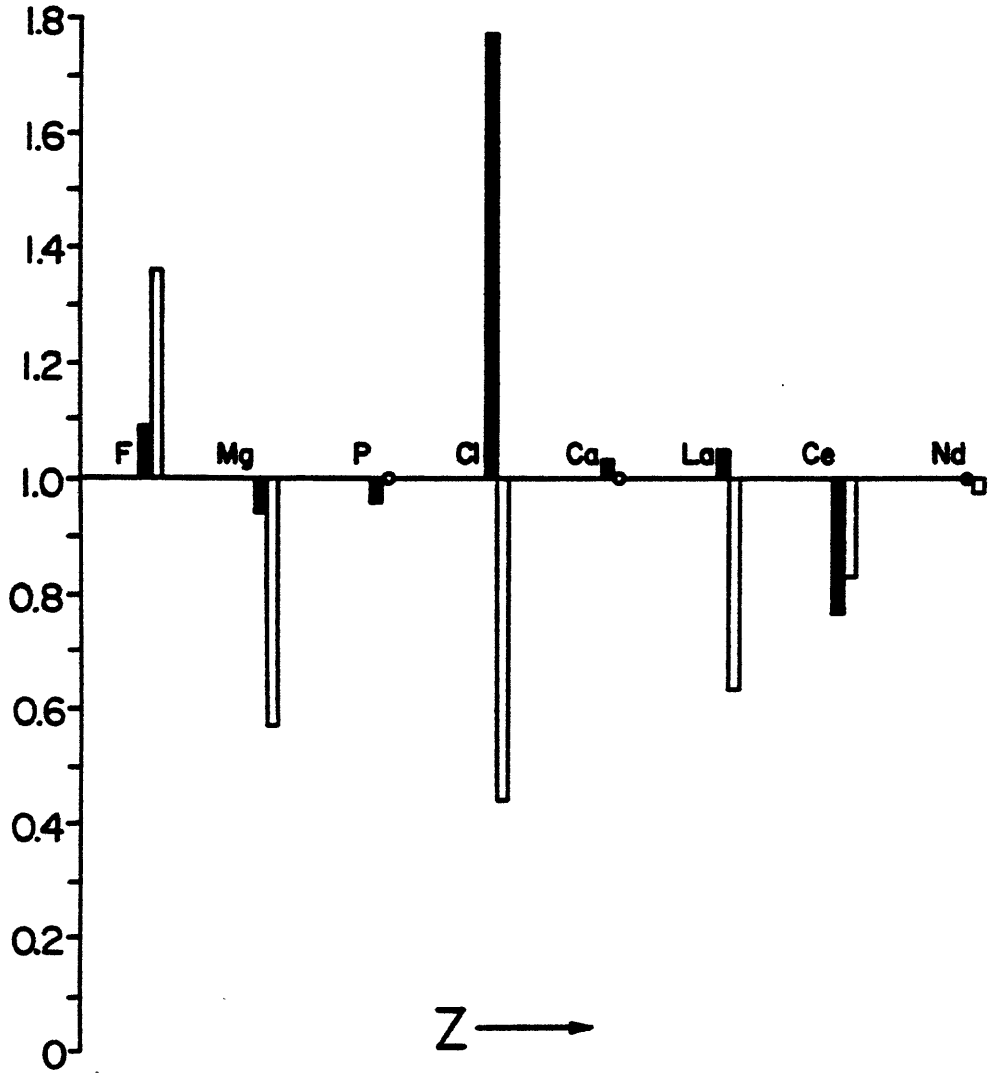

Figure 20.--Enrichment factors (early concentrations/late concentrations) for the apatite from the Joe Lott Tuff Member (black) and the apatite from the Bishop Tuff (clear)
(Hildreth, 1977).

Allanite and chevkinite

Approximately 50 euhedral crystals of dark-reddish-brown and black allanite, a rare-earth rich epidote mineral, and chevkinite, a rare-earth iron titanosilicate, were found in the sample of the basal vitrophyre of the Joe Lott Tuff Member, sample M820. The stubby prisms range in size from 60 to 120 μ in length. Due to the small sample size, 15 of the larger grains were analyzed by electron microprobe, rather than by neutron activation. Both the core and rim of the grains were analyzed, and due to the homogeneity exhibited by the samples, the results were averaged and are given in tables 12 and 13. Levels of F, Na, P, certain REE, and U are below detection limits in the allanite, and Na, P, Mn, some REE, and U are below detection limits in the chevkinite. Five grains were found to be allanite and ten chevkinite.

Spectrum stripping on the microprobe was used to determine the concentrations of the rare-earth elements with particularly severe interference problems. This was done on the following: Nd, Eu, Gd, Tb, Dy, Ho, Er, Tm, Yb, and Lu. Concentrations of Tb through Lu are below limits of detection.

Structural formulae for representative allanites and chevkinites are given in tables 14 and 15. Calculations were based on 2 weight percent H_2O for allanite--an average water content for allanites of similar composition (Deer and others, 1963).

The poor totals of the allanite compositions are perplexing. Comparison of the allanite in the Joe Lott Tuff Member with the Bishop Tuff allanite (Hildreth, 1977) (table 16) shows a close similarity in composition with the exception of the Fe content which is about 6 percent lower in the Joe Lott Tuff Member. An increase of 6 percent Fe would help the totals considerably; however, the chevkinite analyses were determined with microprobe operating conditions similar to the allanite and exhibit totals close to 100 percent. If the Fe is present in a more oxidized state, such as Fe_2O_3, the total would only increase by approximately 1 percent.

The average sum of the REE for the allanite is approximately 21 percent by weight (La+Ce+Pr+Nd+Eu+Gd). This is 60 times greater than the rare-earth concentration (La+Ce) of coexisting zircon and 16 times more than the content of rare earths (Nd+Pr+Ce+La) in coexisting apatite. Relative to coexisting amphibole and pyroxene, allanite is enriched in Al and depleted in Mg and Ca. Allanite is depleted in Y compared to coexisting zircon.

The sum of the REE in the chevkinite averages at about 36 percent by weight (La+Ce+Pr+Nd+Sm+Eu+Gd). This is just over 100 times as much as the coexisting zircon rare-earth content, and 28 times greater than the rare-earth concentration in coexisting apatite. Relative to coexisting amphibole and pyroxene, chevkinite is enriched in Ti and depleted in Fe, Mg, Ca, and, for amphibole only, depleted in Al.

The possibility that the chevkinite may be perrierite was considered. Chevkinite and perrierite have different, yet similar structures and almost identical formulae. The formula for chevkinite is as follows: $A_4BC_4Si_4O_{22}$ where A = REE, Th, Ca, Sr, Na, K; B = Fe^{2+}, Mg, Mn, Ca; and C = Ti, Mg, Mn, Fe^{3+}, Al. By synthesizing chevkinite and perrierite, it was discovered that

Table 12.--Microprobe analyses of allanite in the basal vitrophyre of the Joe Lott Tuff Member

[Analyses given in weight percent. The following elements and oxides are below limit of sensitivity-detection limits in parentheses: F (0.28), Na_2O (0.05), P_2O_5 (0.10), Sm_2O_3 (0.23), Tb_2O_3 (0.16), Dy_2O_3 (0.16), Ho_2O_3 (0.29), Er_2O_3 (0.19), Tm_2O_3 (0.23), Yb_2O_3 (0.23), Lu_2O_3 (0.26), UO_2 (0.50)]

Grain	1	4	11	13	15
SiO_2	27.89	28.24	27.91	26.62	27.44
Al_2O_3	13.11	13.24	13.16	12.14	11.60
TiO_2	1.02	1.57	1.50	1.88	2.46
FeO	10.13	9.87	10.08	10.46	10.29
MgO	1.30	1.78	1.45	1.52	1.41
MnO	.33	.31	.39	.57	.51
CaO	10.62	10.01	10.30	9.47	9.54
Y_2O_3	.58	.30	--	.36	--
La_2O_3	7.98	8.58	9.00	7.92	7.47
Ce_2O_3	13.19	14.11	13.61	13.81	13.47
Pr_2O_3	1.08	.85	.81	1.09	1.23
Nd_2O_3	1.05	2.04	1.01	2.41	2.49
Eu_2O_3	.06	.08	.18	.19	.16
Gd_2O_3	.82	.81	.71	.76	.79
ThO_2	1.60	1.05	1.45	1.71	1.80
Total	90.76	92.84	91.56	90.91	90.66

Table 13.--Microprobe analyses of chevkinite in the basal vitrophyre of the Joe Lott Tuff Member

[Analyses given in weight percent. The following oxides are below limit of sensitivity-detection limits in parentheses: Na_2O (0.05), P_2O_5 (0.10), MnO (0.02), Tb_2O_3 (0.16), Dy_2O_3 (0.16), Ho_2O_3 (0.29), Er_2O_3 (0.19), Tm_2O_3 (0.23), Yb_2O_3 (0.23), Lu_2O_3 (0.26), UO_2 (0.50)]

	2	3	5	6	7	9	12	14	16	17
SiO_2----	19.10	18.56	18.43	17.52	17.08	18.21	16.93	17.07	18.88	17.32
Al_2O_3---	2.84	2.51	2.60	.86	.84	2.67	.78	.89	2.81	2.54
TiO_2----	21.92	17.39	19.92	21.29	21.41	21.59	22.23	20.49	22.45	20.98
FeO-----	4.77	4.96	4.61	6.49	6.48	4.85	6.03	6.02	5.05	4.74
MgO-----	1.05	.91	1.07	.81	.80	.88	.83	.93	.62	.97
CaO-----	5.16	5.18	4.02	3.80	3.67	5.08	3.64	4.02	5.20	5.52
Y_2O_3----	.73	.58	.62	.74	.34	.32	.60	.55	.60	.65
La_2O_3---	12.30	10.70	11.98	10.69	10.88	11.36	11.00	10.06	11.68	10.85
Ce_2O_3---	23.71	22.37	24.72	23.15	22.57	22.84	23.08	22.16	22.60	21.48
Pr_2O_3---	2.22	2.07	2.12	2.11	2.01	2.15	2.07	2.36	2.01	1.70
Nd_2O_3---	6.33	4.84	5.95	6.05	5.63	4.48	3.97	5.42	5.78	5.00
Sm_2O_3---	--	.86	.60	1.03	.42	.52	.38	.89	.43	.44
Eu_2O_3---	.30	.27	.39	.46	.21	.25	.47	.28	.41	.27
Gd_2O_3---	1.80	1.49	1.71	2.06	1.83	1.24	2.00	1.72	1.69	1.57
ThO_2----	.39	4.81	2.18	5.45	7.23	3.21	6.40	8.39	2.95	4.55
F-------	--	.44	.59	--	--	.48	--	--	--	.62
		97.94	101.51			100.13				99.20
O=F-----		.18	.25			.20				.26
Total---	102.62	98.12	101.76	102.51	101.40	100.33	100.41	101.25	103.16	99.46

Table 14.--Structural formulae of representative allanites in the basal vitrophyre of the Joe Lott Tuff Member

[$(REE,Ca,Y)_2$ $(Al_1Fe^{+3})_3$ $(SiO_4)_3(OH)$. Number of ions on basis of 13 (O,OH). Calculations on basis of estimated 2.0 weight percent H_2O]

Grain	11		13	
Si----------	2.925	2.925	2.849	2.849
Al----------	1.626		1.532	
Ti----------	.118		.163	
Fe----------	.883		.936	2.967
Mg----------	.227	2.924	.243	
Th----------	.035		.042	
Mn----------	.035		.051	
Ca----------	1.157		1.086	
Y----------	--	2.128	.021	2.130
REE----------	.971		1.023	
OH----------	1.398	1.398	1.428	1.428

Table 15.--Structural formulae of representative chevkinites in the basal vitrophyre of the Joe Lott Tuff Member

[$A_4BC_4Si_4O_{22}$. A = REE, Th, Ca, Sr, Na, K; B = Fe^{+2}, Mg, Mn, Ca; C = Ti, Mg, Mn, Fe^{+3}, Fe^{+2}, Al. Number of ions on basis of 22 (O,F)]

Grain	9		14	
REE----------	3.113		3.213	
Y----------	.034	4.000	.063	4.100
Th----------	.195		.386	
Ca----------	1.086		.914	
Mg----------	.261	1.000	.291	1.000
Fe----------	.809		1.065	
Ti----------	3.239	4.000	3.262	4.094
Al----------	.628		.222	
Si----------	3.632	3.997	3.613	3.835

Table 16.--Allanite, chevkinite, and perrierite compositions from other localities

[Analyses given in weight percent]

	Allanite Bishop Tuff[1]	Chevkinite Urals[2]	Perrierite Italy[3]
SiO_2	29.69	19.23	19.31
Al_2O_3	10.49	2.17	.67
TiO_2	2.34	19.61	23.24
FeO	16.18	8.75	4.05
Fe_2O_3		2.60	1.26
MgO	.94	.05	.81
MnO	.50	1.11	
CaO	9.09	2.49	4.11
Na_2O	.06	.10	1.05
Y_2O_3	.12	.93	1.51
Nb_2O_5		.01	
La_2O_3	6.97	18.77	6.83
Ce_2O_3	13.04	20.52	31.80
Pr_2O_3	2.48		
Nd_2O_3	3.72		
Sm_2O_3	.42		
ThO_2	.62	.73	4.05
F	.21		
H_2O^+		.81	.61
H_2O^-		.03	
O=F	.09		
Total	96.78	97.91	99.30

[1]Hildreth, 1977.

[2]Vlasov, 1966.

[3]Gottardi, 1960.

the size of the cations filling the A, B, and C sites will determine which structure will form. In the chevkinite structure very large cations can only be accommodated in the A position (Segalstad and Larsen, 1978). Chevkinite and perrierite contain a higher concentration of rare-earth elements, Th, and Ti with a lesser amount of Si, Al, Fe, and Ca than allanite. Comparison of the chevkinite/perrierite of the Joe Lott Tuff Member with microprobe analysis of chevkinite and perrierite from other localities (table 16) indicates that the mineral is indeed chevkinite.

A 114-mm Gandolfi film pattern was made of four grains of chevkinite and allanite by Eugene Foord (U.S. Geological Survey, Denver) (CuK alpha radiation, 35 Kv, 18 ma, 26 hour exposure). The chevkinite appears to be partly metamict as only the four strongest lines for the mineral are present and they are diffuse. The only allanite line found was the strongest one at 9.1 A; therefore, the allanite must have undergone more extensive metamictization than the chevkinite. Perrierite and amphibole lines were looked for but are not visible.

Amphibole

One grain of amphibole was found in the mineral separate containing allanite and chevkinite from the basal vitrophyre of the Joe Lott Tuff Member. The reddish-brown euhedra, 80 μ in length, are difficult to distinguish from the rare-earth minerals. Microprobe analysis and structural formula are given in table 17.

Using the nomenclature of amphiboles compiled by Leake (1978), the sample is a magnesio-hastingsitic hornblende. This nomenclature is used for amphiboles chemically defined with respect to the standard formula $A_{0-1}B_2C_5^{VI*}T_8^{IV}O_{22}(OH,F,Cl)_2$ as follows:

*Roman numerals refer to co-ordination numbers.

$(Ca+Na)_B \geq 1.34$; $Na_B < 0.67$; $(Na+K)_A \geq 0.50$; $Mg/(Mg+Fe^2) \geq 0.70$; Si between 6.25 and 6.49 inclusive; Ti <0.50; $Fe^3 > Al^{VI}$).

Pyroxene

Abundant pale-green pyroxene euhedra are present in all the samples. Larger grains (average 410 μ long) are found in the bottom of the lower and middle units, coinciding well with breaks in the eruptive history. Smaller grains (average 200 μ) are found in the middle and top of the lower unit, top of the middle unit, and the two vitrophyres. Pyroxene in the upper, pink, and bottom of the middle unit is generally somewhat oxidized; only, unaltered grains were selected for microprobe analysis.

Table 17.--Microprobe analysis and structural formula of amphibole in the basal vitrophyre of the Joe Lott Tuff Member

[Analyses given in weight percent]

SiO_2	45.69
Al_2O_3	8.33
TiO_2	1.00
FeO	14.61
MgO	13.78
MnO	.69
CaO	11.81
Na_2O	1.98
K_2O	.76
H_2O	2.00
Total	100.65

$X_{2-3}Y_5Z_8O_{22}(OH,F,Cl,O)_2$. X = Ca, Na, K, Mn; Y = Mg, Fe^{+2}, Fe^{+3}, Al, Ti, Mn, Cr, Li, Zn; Z = Si, Al. Number of ions on basis of 24(O,OH)

Si	6.741	8.190
Al	1.449	
Ti	.111	
Fe	1.802	4.943
Mg	3.030	
Mn	.086	
Ca	1.867	2.663
Na	.566	
K	.144	
OH	1.968	1.968

A core and rim analysis was made on five grains from each sample. The compositions are so similiar that the results were averaged for each sample and, along with the structural formulae, are given in table 18. Table 19 lists the calculated end members (Fe and Mn values assigned to ferrosilite) which are plotted on a ternary diagram (fig. 21). Samples from the Joe Lott Tuff Member and crystal-rich tuff member exhibit little compositional variation and plot in the augite field with the exception of M828 (middle of the lower unit) which is endiopside. Augite composition ranges from $Wo_{45}En_{45}Fs_{10}$ to $Wo_{40}En_{43}Fs_{17}$. The varying concentration of the iron appears to be the main cause of the compositional range; however it appears to change at random with little regard to the cooling breaks.

GEOTHERMOMETRY

The distribution of temperatures within the pre-eruptive magma chamber can be constrained by several methods. The post-emplacement oxidation of the iron-titanium oxides in the Joe Lott Tuff Member precluded the application of the iron-titanium oxide geothermometer of Buddington and Lindsley (1964). Three other geothermometers were applied to the Joe Lott Tuff Member.

Figure 22 shows the liquidus surface for water-saturated $NaAlSi_3O_8$-$KAlSi_3O_8$-SiO_2 systems at 1,000 bars confining pressure. The boundary curve wqms separates the quartz from the feldspar field, and m is the isobaric minimum. Isotherms show the configurations of the liquidus surface. All liquids which begin crystallization in the field $NaAlSi_3O_8$-w-q-M become more potassic with cooling, as do their feldspars, by leaving more albitic feldspars behind. The unique fractionation curve qM divides this field from the area $KAlSi_3O_8$-m′-m-s. Liquids and feldspars in the latter area, on the other hand, become more sodic during crystallization. Feldspars crystallized out of liquids which fall into the field M-q-m-m′ first become more sodic, and then both liquid and feldspar become more potassic.

The Joe Lott Tuff Member chemical data can be modeled in terms of experimental systems to constrain the temperatures and pressures present in the pre-eruptive magma chamber. The vitrophyre contains only about one percent crystals, thus confining the system in P-T space essentially to the liquidus. This, combined with the low CaO content and the high differentiation index (Thorton and Tuttle, 1960) allows one to model the data in the system Q-Ab-Or, with some assumptions. A fluid pressure of 1 kb is reasonable for a first approximation model of the conditions within the Mount Belknap magma chamber. The normative salic constituents in the samples from the Joe Lott Tuff Member and the crystal-rich tuff member are plotted in figure 8. Most of the samples cluster near the thermal trough with the exception of the crystal-rich tuff member (M672) and the pink unit (M832). The crystal-rich tuff member unit has markedly different chemistry from the Joe Lott Tuff Member. The basal vitrophyre of the Joe Lott Tuff Member has a bulk composition that lies in the thermal trough and is closest to the minimum. No systematic change in composition is seen relative to stratigraphic position.

The temperatures of formation obtained from the Q-Ab-Or ternary diagram are shown in table 20. A systematic increase in temperatures is seen from the basal vitrophyre through the top of the lower cooling unit as successively deeper levels of the magma chamber are tapped.

Table 18.--Microprobe analyses of representative pyroxene in the Joe Lott Tuff Member and the crystal-rich tuff member

[Analyses given in weight percent. K_2O and Cr_2O_3 are below detection unit of 0.01 and 0.02 weight percent, respectively]

	M820		M827		M828		M829		M830		M831		M832		M833		M672	
SiO_2---	50.95		48.16		52.36		49.88		52.02		51.17		52.13		51.76		49.08	
Al_2O_3--	2.36		4.86		2.45		3.66		1.42		4.42		3.07		2.15		2.53	
TiO_2---	.88		1.30		.33		.51		.40		1.16		.94		.98		.77	
FeO----	10.36		8.51		4.25		6.42		8.44		7.04		9.59		10.10		8.04	
MnO----	.45		.24		.09		.18		1.28		.18		.16		.33		.99	
MgO----	15.54		15.52		17.33		16.37		14.91		15.91		15.07		15.44		14.98	
CaO----	19.52		20.56		21.77		21.67		21.05		20.99		20.08		19.87		21.08	
Na_2O---	.53		.71		.89		.40		.88		.68		.81		.61		.92	
Total--	100.59		99.86		99.47		99.09		100.40		101.55		101.85		101.24		98.39	
Formulae calculated on basis of 6 oxygens																		
Si-----	1.899	2.000	1.805	2.000	1.921	2.000	1.863	2.000	1.941	2.000	1.858	2.000	1.905	2.000	1.912	2.000	1.874	2.000
Al-----	.103		.215		.106		.162		.062		.167		.132		.094		.114	
Ti-----	.025		.037		.009		.014		.012		.032		.026		.028		.022	
Fe-----	.323	2.046	.267	2.078	.131	2.037	.201	2.055	.264		.214		.293		.312		.257	
Mn-----	.014		.008		.003		.006		.040	2.051	.006	2.004	.005	2.026	.010	2.036	.032	2.083
Mg-----	.864		.868		.948		.912		.829		.862		.821		.850		.853	
Ca-----	.780		.826		.856		.868		.839		.817		.787		.787		.863	
Na-----	.038		.052		.063		.029		.064		.048		.057		.043		.068	

Table 19.--Pyroxene end members in the Joe Lott Tuff Member and the crystal-rich tuff member

Sample	Description	X_{WO}	X_{EN}	X_{FS}
M672	Crystal-rich tuff member, vitrophyre----------	42.30	42.52	15.18
	Joe Lott Tuff Member			
M833	Upper unit----------	40.41	43.00	16.59
M832	Pink unit----------	40.96	43.45	15.59
M831	Middle unit - top----------	43.73	45.31	10.96
M830	Middle unit - bottom-------	42.26	42.90	14.84
M829	Lower unit - top----------	44.72	44.93	10.35
M828	Lower unit - middle--------	44.91	48.75	6.34
M827	Lower unit - bottom--------	40.86	43.80	15.34
M820	Vitrophyre----------	41.58	43.96	14.46

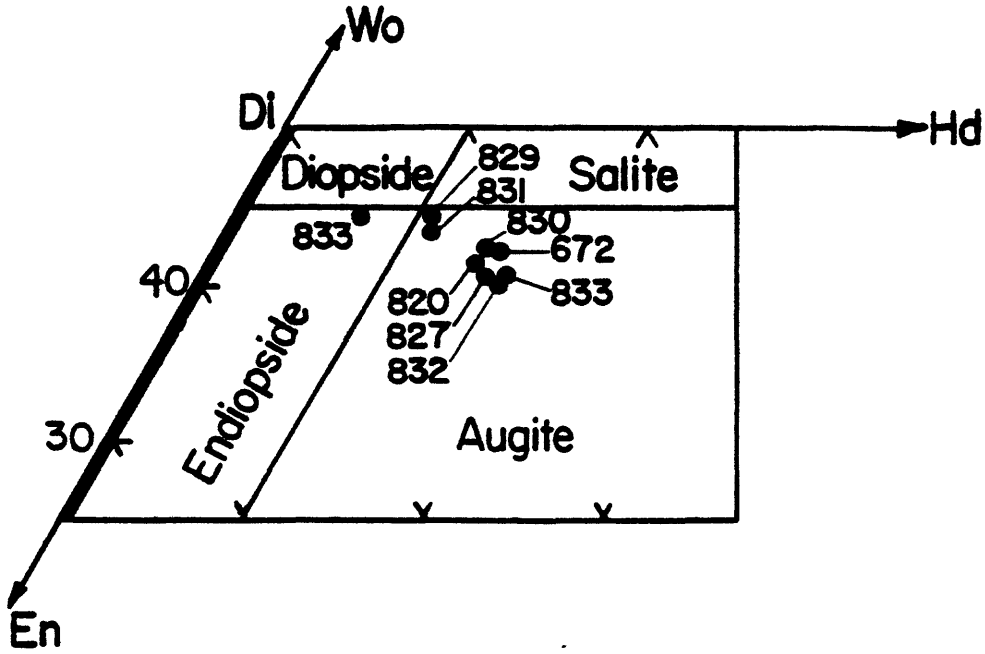

Figure 21.--Composition and nomenclature of the pyroxene in the Joe Lott Tuff Member and the crystal-rich tuff member.

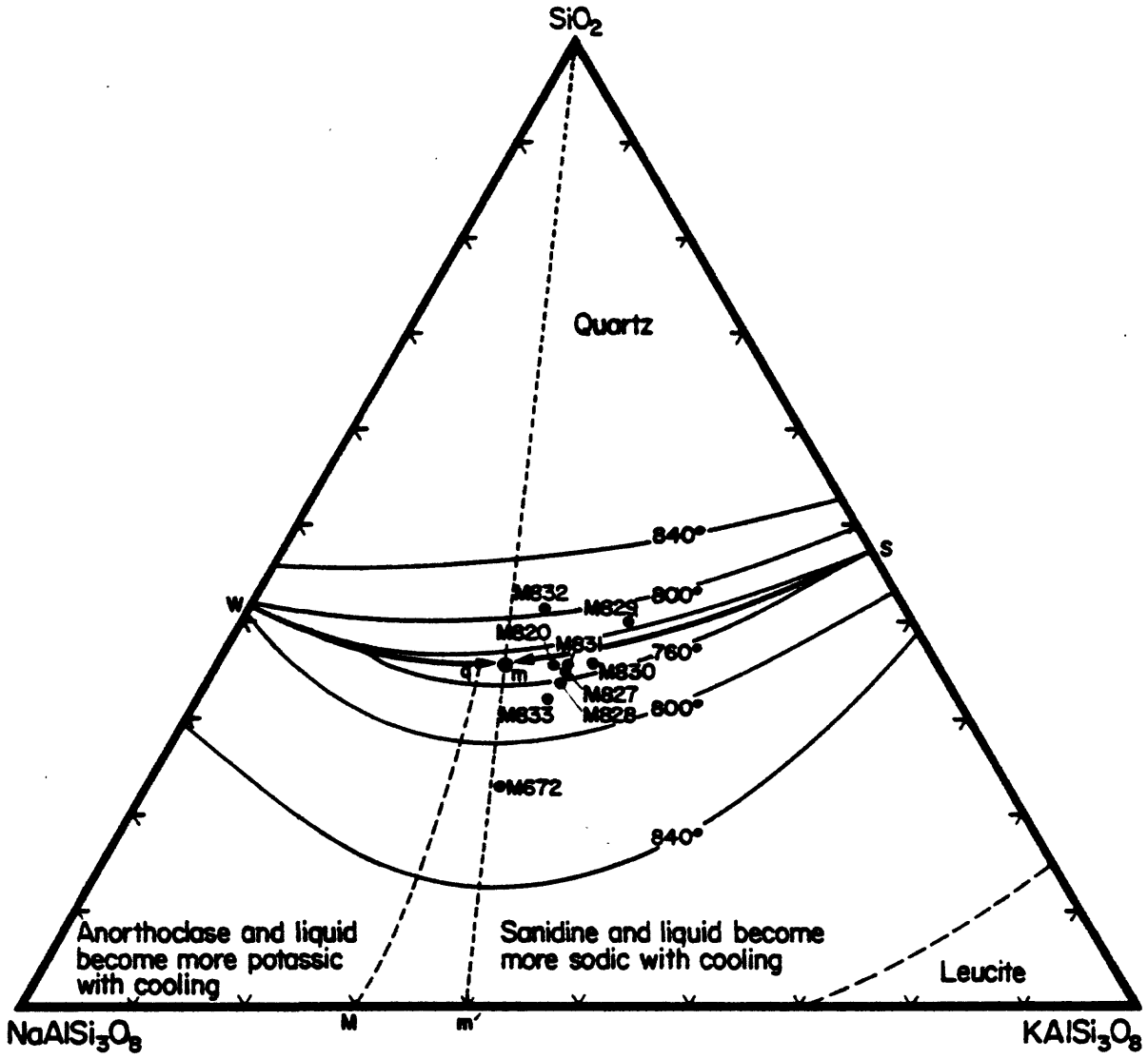

Figure 22.--Liquidus surface for water-saturated liquids at 1,000 bars confining pressure in the system $NaAlSi_3O_8$-$KAlSi_3O_8$-SiO_2 showing the Joe Lott Tuff Member and the crystal-rich tuff member salic normative compositions (modified from Carmichael and others, 1974). Temperature in ^oC.

Table 20.--Temperatures of formation of the Joe Lott Tuff Member and the crystal-rich tuff member obtained by three different methods

Sample	Temperature in °C			
	Feldspar geothermometer (fig. 24)	Q-Ab-Or (fig. 22)	Ab-Or-An (fig. 23)	
			Sanidine	Plagioclase
Crystal-rich tuff member,				
vitrophyre----------	900°	810°	835°	700°
Joe Lott Tuff Member				
upper unit----------	770°	725°		
pink unit----------	740°	800°	725°	
middle unit - top-----	740°	750°	770°	
middle unit - bottom--	650°	760°		
lower unit - top------	700°	770°	750°	
lower unit - middle---	620°	760°		
lower unit - bottom---	780°	760°	800°	
vitrophyre----------	780°	750°		

Sanidine and plagioclase compositions from microprobe data are plotted on Seck's (1971) ternary diagram in figure 23. Tie lines are drawn between coexisting pairs of sanidine and plagioclase showing their relationship to cooling units. Temperatures of formation can be obtained for five Joe Lott Tuff Member sanidine samples and the crystal-rich tuff member feldspars whose compositions fall within the bounds of Seck's experimentally derived temperature data. They are listed in table 20.

Potassium feldspar from the basal vitrophyre of the crystal-rich tuff member (M672) yielded an average composition of An:4.4, Ab:57.5, Or:38.1--which corresponds, on Seck's diagram, to a temperature of 825°C. This is somewhat higher than the temperatures found for the other samples of the crystal-rich tuff member, M74 and M75, which indicate temperatures of 650°C and 750°C, respectively. The differences may result from the fact that the samples were collected from three widely different locations and reflect different depths in the magma chamber.

A two feldspar geothermometer developed by Stormer (1975) was also used to model the microprobe data. This geothermometer employs the concept of the partitioning of the albite component in equilibrium plagioclase and alkali feldspar pairs. As little variation between core and rim compositions in the Joe Lott Tuff Member feldspar was observed, mean compositions were used for the geothermometer. Curves relating temperature to albite composition at given pressures have been generated by Stormer. A pressure of 1,000 bars was again used for the samples from the Joe Lott Tuff Member and crystal-rich tuff member.

The temperatures determined by the Stormer (1975) geothermometer for the thin section feldspar compositions are plotted in figure 24. The basal vitrophyre and the bottom of the lower unit give a temperature of formation of about 780°C. The middle of the lower unit has a lower temperature of approximately 620°, perhaps coinciding with the discontinuity observed in the chemical data at this stage, and then temperature increases with depth in the magma chamber to 700° at the top of the lower unit. Temperature drops slightly to 650° with the break in eruption between the lower and middle cooling units and increases with depth to 740°C when the top of the middle cooling unit is emplaced. The pink unit also gives a temperature of formation of 740°C perhaps indicating eruption soon after the middle unit. The crystal-rich tuff member feldspars indicate a high temperature of formation of approximately 900°C; however, the albite components plot in the area outside of the solid lines.

The temperatures of feldspar formation obtained by this method and the two already discussed are in table 20. The temperatures derived from the first two methods vary somewhat from those obtained from the two-feldspar geothermometer; however, overall trends are roughly comparable. The primary discrepancy lies in the temperatures of the lower cooling unit which increase systematically with depth using the Q-Ab-Or geothermometer; however, temperatures decrease and then rise again midway through the lower unit using Stormer's geothermometer.

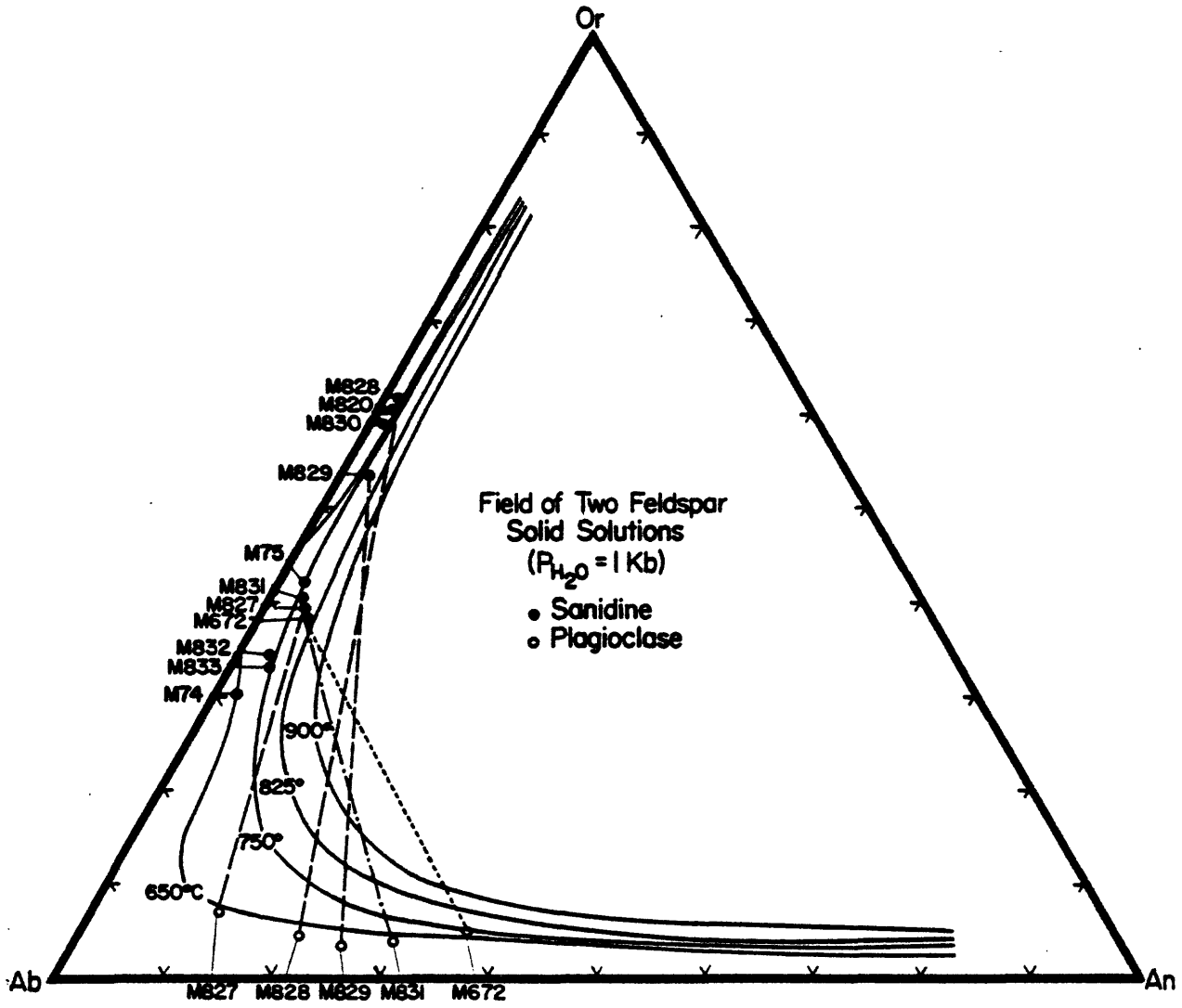

Figure 23.--Feldspar compositions in weight percent Ab, Or, and An of the Joe Lott Tuff Member and the crystal-rich tuff member shown in Seck's (1971) experimental temperature data. Tie lines drawn between coexisting sanidine (.) and plagioclase (o) pairs as follows:
crystal-rich tuff member, vitrophyre - short dashes
Joe Lott Tuff Member
middle cooling unit - dash, dot, dash
lower cooling unit - long dashes

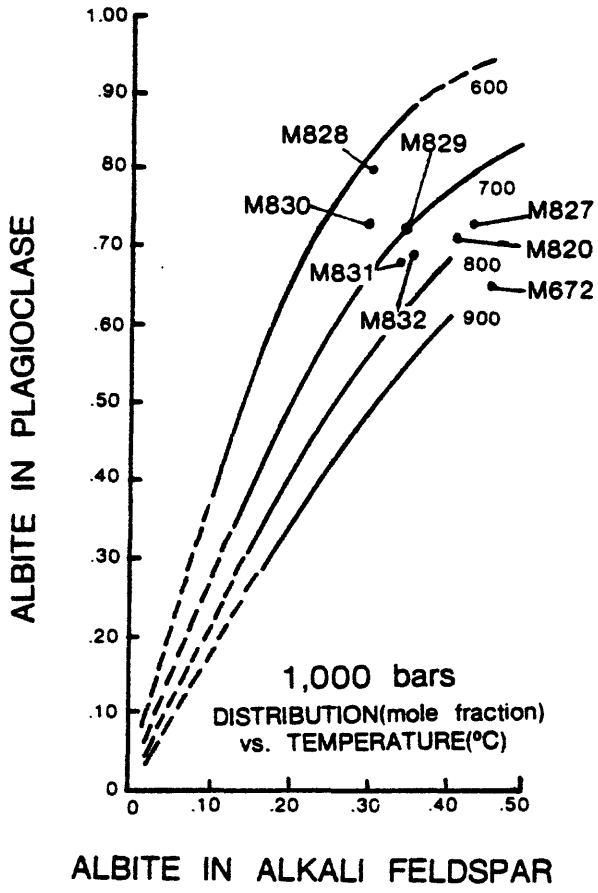

Figure 24.--Determinative curves for temperature based on the model of albite distribution between coexisting plagioclase and alkali feldspars (modified from Stormer, 1975). Compositions of coexisting pairs of feldspars in the thin sections of the Joe Lott Tuff Member and the crystal-rich tuff member are shown.

ORIGIN OF THE COMPOSITIONAL ZONATION

There are several lines of evidence which indicate that the Joe Lott Tuff Member was erupted from one volume of magma. Field relations such as the lack of erosion, channeling, or other deposits between cooling units distal to the caldera imply that the ash flow was erupted within a fairly short time; however, rhyolite lava flows interleaved with the tuff near the source demonstrate the intermittent character of the eruption. Further evidence includes the overall chemical homogeneity of the tuff, particularly as exhibited by the major elements, and the consistent phenocryst assemblage throughout the units, with slight variation in the basal vitrophyre. A fairly systematic increase in phenocryst content and temperature is found upward in each cooling unit and is believed to reflect their derivation from deeper source levels in the magma chamber. Variation in silica content is minor in the Joe Lott Tuff Member averaging about 76 weight percent. The crystal-rich tuff member which has its source deep in the chamber, has SiO_2 = 71.44 weight percent.

The primary compositional variations which should be accounted for by a fractionation model include the following: (1) the trends exhibited by many elements vertically through each separate cooling unit of the ash flow. In the whole-rock data, trends are evident in Si, K, U, Li, Mo, and Nb. (2) The majority of elements in the enrichment/depletion diagram (fig. 9) are enriched, reflecting a higher concentration in the early erupted material than in the later erupted portion. Of note is the extreme enrichment of Cs and, to a slightly lesser extent, Mo, H_2O, and Co, along with the depletion of Sb. Also noteworthy is the antithetic behavior of Na and K, and the enrichment of all the REE from La through Yb. (3) Despite the variations in elemental content illustrated by the aforementioned patterns, the whole-rock and mineralogical data do not vary a great deal overall indicating that the magma was fairly homogeneous, particularly in the major elements. All minor and trace elements detected exhibit more pronounced gradients. (4) The temperature of formation increases upward in each cooling unit; however, a break in the pattern is seen in the lower cooling unit with Stormer's geothermometer.

Fractional Crystallization

There is a multitude of evidence that argues against fractionation by crystal settling in the Joe Lott Tuff Member, which closely parallels the reasoning done by Hildreth (1977, 1979, 1981) in his analysis of the compositional zonation found in the Bishop Tuff. Zircon, the dense, earliest crystallized mineral, is present as unzoned, euhedral crystals throughout the Joe Lott Tuff Member and thus did not settle to any great extent. Zircon is known to crystallize early in a cooling rhyolitic magma. The distribution of the larger pink zircons and the smaller clear grains would have been affected by their different settling velocities; however, the amount of both species changes little per sample. Also, little variation is seen in the Zr and Si content of zircon at different levels of the tuff.

Crystal settling does not seem to have had any effect on the apatite either. The crystals vary in size by a factor of two and the complete size spectrum is found throughout the vertical extent of the tuff. The P and Ca concentrations of the apatite are markedly uniform.

Allanite and chevkinite, second only to zircon in density, were present solely in the top of the magma chamber. The same holds true for the hornblende, and certainly does not lend much credence to crystal settling. The larger (400 μ) phenocrysts of pyroxene are present in the bottom of both the lower and middle cooling units, whereas the tops of these units contain the smaller (200 μ) variety of grains, again arguing against crystal settling.

The whole-rock K_2O content increases even though the relative percent of sanidine versus plagioclase decreases upward in the lower cooling unit implying no K_2O enrichment from feldspar accumulation, and magmatic zonation prior to phenocryst precipitation.

Although a greater amount of most minor and rare earth elements is found in the early erupted samples, the elements are present in the apatite and zircon throughout the tuff; thus crystal settling did not control their fractionation. If the strong enrichment seen in the Joe Lott Tuff Member was caused by crystal fractionation, it would have been necessary for an unreasonable proportion of the magma to have crystallized. The low (<1%) phenocryst content of the Joe Lott Tuff Member indicates the proximity to the liquidus; therefore, the minor number of phenocrysts able to crystallize did not have time to settle far prior to eruption.

Convection-Driven Thermogravitational Diffusion

As a result of the recent work by Shaw and others (1976) and Hildreth (1976, 1977, 1979, 1981) primarily on the Bishop Tuff, California, thermogravitational diffusion is becoming an increasingly better understood mechanism of fractionation in high-silica magma chambers. Geochemical studies on the outflow from comparable siliceous systems yield compositional zonations strikingly similar to those found in the Bishop Tuff. Analogy with the Bishop Tuff was seen in the major, minor, and trace element behavior in the Bandelier Tuff, New Mexico (Smith, 1979); Sierra La Primavera, Jalisco, Mexico (Mahood, 1981); Coso Volcanic Field, California (Bacon, 1981); and Twin Peaks, Utah (Crecraft and others, 1981). The chemical gradients, which cannot be explained by crystal fractionation, can easily be accounted for with thermogravitational diffusion.

The thermogravitational diffusion model set forth by Shaw and others (1976) explains the cycles of related compositional, volatile, and thermal gradients found in large-volume silicic magma chambers. The model emphasizes the combined effects of convective circulation and the Soret effect to generate the chemical gradients in the zoned upper parts of magma chambers. Soret diffusion is the spontaneous growth of concentration gradients in liquid and gaseous systems until a steady-state distribution is attained. The gradients remain until the decay of the thermal gradient.

The mechanics of the thermogravitational diffusion model have been expanded on by Hildreth (1977, 1979, 1981) as a result of his work on the Bishop Tuff, and are outlined below. Intrusion of basaltic magma into the crust initiates and maintains partial melting of the crust creating a shallow silicic magma chamber. The additional heat of the intruding basalt causes the magma to convect. A rising boundary layer, enriched in volatile components and metals that form complexes with them, moves upward at the interface of the convecting magma and the wall rocks in response to the temperature gradient and forms a gravitationally stable roof-zone magma. The most pronounced

enrichments and depletions are present in the roof of the magma chamber resulting from the combined effects of the thermal gradient, the presence of water and other volatiles, the formation of ionic complexes, and variations in polymerization of the melt. The upward enrichment of dissolved volatiles lowers the liquidus temperature decreasing the phenocryst content in the roof of the magma chamber. Convective remixing of the zoned upper magma is prevented by a volatile-concentration gradient. The high-silica roof zone increases in size at the expense of the convecting dominant volume of magma beneath it. The gradients within the stable zone are strengthened by this diffusive exchange with the subjacent magma, by internal diffusion, or by the input of water from the country rocks. The chemical evolution of the open magmatic system is also affected by the changing thermal conditions, by crystal-liquid fractionation, and intermittently by intrusions of primitive magma into the root zone which intensifies the convective circulation and transport of volatiles roofward in the shallow chamber.

The repeated establishment of minor-element gradients in a stable roof zone has been documented by two major ash-flow eruptions in the Bandelier Tuff (Smith, 1979). The gradients are interpreted to reflect the changing boundary-layer conditions at the roof of the magma chamber caused by the temperature and volatile gradients between the roof and the subjacent convecting body. The presence of similar chemical gradients in both ash flows indicates the re-establishment of the convecting and differentiating system between eruptions.

The pattern of chemical gradients seen in the lower cooling unit and again in the middle unit of the Joe Lott Tuff Member, along with the marked enrichment of almost all the elements in the early erupted samples, are much more easily explained by differentiation in the liquid state by thermogravitational diffusion than by fractional crystallization. The roofward decrease in degree of crystallization as well as temperature in the Mount Belknap magma chamber indicates the roofward enrichment of water and halogens. Inasmuch as the halogen content of the Joe Lott Tuff Member is low, it appears that the fluctuating water content was more instrumental in the development of a zoned stable high-silica roof zone. The higher fluorine and chlorine content of the early relative to the later erupted apatite indicates an increase in halogen content in the upper part of the roof zone. As recurrence intervals of as short as 0.3 m.y. (Smith, 1979) are known for similar large-volume high-silica systems, the repeated gradients observed in the lower and middle cooling units are not inconsistent with the model. Volatiles derived from new pulses of basic magma would establish the renewed gradients.

The discontinuity of some of the minor element variation patterns halfway through the eruption of the lower cooling unit puts severe time constraints on the model which may be unreasonable. Discontinuous enrichment or depletion in the lower cooling unit is seen in Si, K, U, Li, Mo, and Nb in the whole-rock data; in the Or and Ab content of the sanidine; in the Y content of the clear zircons; and in P, Mg, Nd, Ce, and La in the apatite.

These repeated cycle of chemical gradients may not reflect the fractionation of two separate pulses of magma, but rather the rise and re-equilibration of the magma left in the chamber after the initial collapse of the roof rocks and the primary eruption. A new boundary layer could develop out of the nonequilibrium conditions present in the magma chamber after

partial eruption, re-establishing the gradients existing prior to the eruption. The high phenocryst content in the top of the lower cooling unit implies that some crystallizing magma remained in the chamber after the first eruption. This re-stratification of the magma may require a greater time break than field evidence allows.

The topographic wall of the Mount Belknap caldera outlines two distinct lobes (fig. 1), rather than a regular outline. The repeated gradients in the lower cooling unit may result from the irregular evacuation of a compositionally zoned magma chamber. An initial eruption may have formed one lobe of the caldera and one cycle of gradients. The remaining stratified magma subsequently filled in the cavity and erupted, completing the formation of the lower unit and causing the second cycle of gradients. The cooler temperature in the middle of the lower unit and subsequent rise in the top of the lower unit found with the Stormer geothermometer substantiate this relatively short break in eruptive history.

The enrichment and depletion trends seen in the Joe Lott Tuff Member are comparable to those found in the Bishop Tuff (Hildreth, 1981) and from some other similar studies. The modest gradients exhibited by the major elements is a common trait. In the Joe Lott Tuff Member, the intensity of REE enrichment increases from La through Tb then drops off to a slight depletion in Lu. Enrichment patterns for other high-silica volcanic systems commonly exhibit REE crossover behavior from lessening depletion to increasing enrichment between Nd and Sn, with an Eu depletion attributable to removal by feldspars. The presence of the LREE-rich minerals allanite and chevkinite found exclusively in the basal vitrophyre--the top of the magma chamber--is explained by the enrichment of the LREE in the Joe Lott Tuff Member samples. Allanite is a far more efficient concentrator of LREE than apatite and sphene (Miller and Mittlefehldt, 1982) which are present throughout the Joe Lott Tuff Member samples. The microprobe analyses showed the allanite and chevkinite to be 16 times and 28 times, respectively, more enriched in REE than coexisting apatite. The behavior of Si, Al, Ti, and Fe^{3+} in rhyolitic melts and their resulting gradients in zoned magmas is not entirely understood (Hildreth, 1981). Strong enrichment is usually seen for the highly charged (>3+) elements and is caused by thermogravitational transport as a volatile complex. Few stable sites exist for the highly charged species in the strongly polymerized silicate melts, forcing their movement to the less-polymerized roof zone of the magma chamber (Hildreth, 1981). This accounts for the marked Mo enrichment, along with U, Th, and Nb, in the Joe Lott Tuff Member. Other elemental trends found in the high-silica volcanic systems studied, which have undergone differentiation in the liquid state by thermogravitational diffusion, are the upward enrichments of Na, Li, Rb, and Cs, all being antithetic to K. This is seen in the Joe Lott Tuff Member samples, particularly strongly in Cs. Upward enrichment is seen in the Joe Lott Tuff Member for the first transition series metals--Sc, Ti, Cr, Fe, and Co. Similar behavior in the Bishop Tuff is only seen for Sc. The depletion of Zr and the stable Hf content throughout the eruption of the Joe Lott Tuff Member is a common result of thermogravitational diffusion.

The intrusion of basalt into the crust is thought to initiate and sustain convection-driven thermogravitational diffusion. The high heat flow associated with the bimodal basalt-rhyolite volcanism resulting from the changeover to an extensional tectonic regime in the Marysvale Volcanic Field is well suited to the model.

REFERENCES

Bacon, C. R., 1981, Pleistocene high-silica rhyolites of the Coso Volcanic Field, Inyo County, California: Journal of Geophysical Research, v. 86, no. B11, p. 10223-10241.

Buddington, A. F., and Lindsley, D. H., 1964, Iron-titanium oxide minerals and synthetic equivalents: Journal of Petrology v. 5, no. 2, p. 310-357.

Carmichael, I. E., Turner, F. J., and Verhoogen, John, Igneous Petrology, McGraw-Hill Book Company, 1974, 739 p.

Crecraft, H. R., Nash, W. P., and Evans, S. H., Jr., 1981, Late Cenozoic volcanism at Twin Peaks, Utah: Geology and Petrology: Journal of Geophysical Research, v. 86, no. B11, p. 10303-10320.

Cunningham, C. G., Ludwig, K. R., Naeser, C. W., Weiland, E. K., Mehnert, H. H., Steven, T. A., and Rasmussen, J. D., 1982, Geochronology of hydrothermal uranium deposits and associated igneous rocks in the eastern source area of the Mount Belknap Volcanics, Marysvale, Utah: Economic Geology, v. 77, no. 2, p. 444-454.

Cunningham, C. G., and Steven, T. A., 1979, Mount Belknap and Red Hills Calderas and associated rocks, Marysvale Volcanic Field, west-central Utah: U.S. Geological Survey Bulletin 1468, 34 p.

Cunningham, C. G., Steven, T. A., and Naeser, C. W., 1982, Multiple episodes of igneous activity, mineralization, and alteration in the western Tushar Mountains, Utah: U.S. Geological Survey Open-File Report 82-479, 16 p.

Dalrymple, G. B., and Lanphere, M. A., 1969, Potassium-Argon Dating: W. M. Freeman and Company, San Francisco, 258 p.

Deer, W. A., Howie, R. A., and Zussman, J., 1963, Rock-Forming Minerals, v. 4, Framework Silicates: Longmans, Green and Co., Ltd., London, 435 p.

Drake, M. J., and Weill, D. F., 1972, New rare earth element standards for electron microprobe analysis: Chemical Geology, v. 10, no. 2, p 179-181.

Effinroff, I., 1972, The chemical and morphological variations of zircons from the Boulder Batholith, Montana: unpublished PhD. thesis, University of Cincinnati, Cincinnati, Ohio, 136 p.

Gottardi, G., 1960, The crystal structure of perrierite: American Mineralogist, v. 45, no. 1-2, p. 1-14.

Hildreth, W., 1976, The Bishop Tuff: Compositional zonation in a silicic magma chamber without crystal settling (abs.): Geological Society of America Abstracts with Programs, v. 8,p. 918.

Hildreth, E. W., 1977, The magma chamber of the Bishop Tuff: Gradients in temperature, pressure, and composition: unpublished PhD. thesis, University of California, Berkeley, California, 328 p.

Hildreth, W., 1979, The Bishop Tuff: Evidence for the origin of compositional zonation in silicic magma chambers: Geological Society of America Special Paper 180, p. 43-75.

Hildreth, W., 1981, Gradients in silicic magma chambers: Journal of Geophysical Research, v. 86, no. B11, p. 10153-10192.

Leake, B. E., 1978, Nomenclature of amphiboles: American Mineralogist, v. 63, no. 11-12, p. 1023-1052.

Lipman, P. W., 1965, Chemical comparison of glassy and crystalline volcanic rocks: U.S. Geological Survey Bulletin 1201-D, p. 29-39.

Lipman, P. W., Christiansen, R. L., and O'Connor, J. T., 1966, A compositionally zoned ash-flow sheet in southern Nevada: U.S. Geological Survey Professional Paper 524-F, 47 p.

Ludington, S., 1981, The Redskin Granite--evidence for thermogravitational diffusion in a Precambrian granite batholith: Journal of Geophysical Research, v. 86, no. B11, p. 10423-10430.

Mahood, G. A., 1981, A summary of the geology and petrology of the Sierra La Primavera, Jalisco, Mexico: Journal of Geophysical Research, v. 86, no. B11, p. 10137-10152.

Miller, C. F., and Mittlefehldt D. W., 1982, Depletion of light rare-earth elements in felsic magmas: Geology, v. 10, no. 3, p. 129-133.

Millot, G., 1970, Geology of Clays: Springer-Verlag, N. Y., 429 p.

Rowley, P. D., Steven, T. A., and Mehnert, H. H., 1981, Origin and structural implications of upper Miocene rhyolites in Kingston Canyon, Piute County Utah: Geological Society of America Bulletin, Pt. I, v. 92, no. 8, p. 590-602.

Seck, H. A., 1971, Alkali feldspar-liquid and alkali feldspar-liquid-vapor relationships at pressures of 5 and 10 kbar: Neues Jahrbuch fur Mineralogie Abhandlungen, v. 115, no. 2, p. 140-163.

Segalstad, T. V., and Larsen, A. O., 1978, Chevkinite and perrierite from the Oslo region, Norway: American Mineralogist, v. 63, no. 5-6, 499-505.

Shaw, H. R., Smith, R. L., and Hildreth, W., 1976, Thermogravitational mechanisms for chemical variations in zoned magma chambers (abs.): Geological Society of America Abstracts with Programs, v. 8, p. 1102.

Smith, R. L., 1979, Ash-flow magmatism: Geological Society of America Special Paper 180, p. 5-27.

Smith, R. L., and Bailey, R. A., 1966, The Bandelier Tuff: A study of ash-flow eruption cycles from zoned magma chambers: Bulletin Volcanologique, ser. 2, v. 29, p. 83-104.

Steven, T. A., Cunningham, C. G., Naeser, C. W., and Mehnert, H. H., 1979, Revised stratigraphy and radiometric ages of volcanic rocks in the Marysvale area, west-central Utah: U.S. Geological Survey Bulletin 1469, 40 p.

Stormer, J. C., Jr., 1975, A practical two-feldspar geothermometer: American Mineralogist, v. 60, no. 7-8, p. 667-674.

Stuckless, J. S., and VanTrump, G., Jr., 1979, A revised version of graphic normative analysis program (GNAP) with examples of petrologic problem solving: U.S. Geological Survey Open-File Report 79-1237, 112 p.

Tuttle, O. F., and Bowen, N. L., 1958, Origin of granite in the light of experimental studies in the system $NaAlSi_3O_8$-$KAlSi_3O_8$-SiO_2-H_2O: Geologic Society of America Memoir 74, 153 p.

Thorton, C. P., and Tuttle, O. F., 1960, Differentiation index [Pt.] 1, of Chemistry of igneous rocks: American Journal of Science, v. 258, no. 9, p. 664-684.

Vlasov, K. A., (editor), 1966, Geochemistry and mineralogy of rare elements and genetic types of their deposits, v. 2, Mineralogy of rare elements: Israel Program for Scientific Translations, Jerusalem, p. 309-312.

Washington, H. S., 1917, Chemical analyses of igneous rocks published from 1884 to 1913, inclusive: U.S. Geological Survey Professional Paper 99, 1201 p.

Wright, T. L., 1968, X-ray and optical study of alkali feldspar--[Pt.] 2, An X-ray method for determining the composition and structural state from measurement of 2θ values for three reflections: American Mineralogist, v. 53, no. 1-2, p. 88-104.